ELSEVIER

International Journal of Mass Spectrometry 178 (1998) 81–112

International Journal of Mass Spectrometry

Measurement of light stable isotope ratios by SIMS: Matrix effects for oxygen, carbon, and sulfur isotopes in minerals

Lee R. Riciputi*, Bruce A. Paterson[1], Robert L. Ripperdan[2]

Chemical and Analytical Sciences Division, Oak Ridge National Laboratory, Oak Ridge, TN 37831-6365, USA

Received 24 December 1997; accepted 23 June 1998

Abstract

Mass bias occurring during analysis of the light stable isotopes of oxygen, carbon, and sulfur in geological materials by secondary ionization mass spectrometry has been investigated. The effects of instrumental parameters (primary ion beam, secondary ion energy, and polarity) were evaluated by measuring sulfur isotope ratios in conductive sulfide minerals. The role of analyte chemical composition (matrix effect) on mass bias was investigated in sulfides (sulfur), silicates and oxides (oxygen), and carbonates (oxygen and carbon). For oxygen and carbon, various correlations between mass bias and matrix parameters have been identified. The application of several empirical models for prediction of oxygen isotopic mass bias indicates that for silicates, depending on mineral composition, bias can be predicted with an accuracy that is typically within two times that of the precision. However, extension of these models to other matrices has proved problematic, indicating that additional factors are important. (Int J Mass Spectrom 178 (1998) 81–112) © 1998 Elsevier Science B.V.

Keywords: Secondary ion mass spectrometry; Ion microprobe; Isotope ratios; Mass bias; Matrix effects; Oxygen; Carbon; Sulfur

1. Introduction

In recent years, secondary ion mass spectrometry (SIMS, or ion microprobe) has been increasingly used for the analysis of light stable isotope ratios in geological and cosmochemical studies [e.g. 1–7]. The ion microprobe provides the capability of resolving fine-scale (<50 μm) isotopic variations within single mineral grains and analyzing fine-grained minerals without the need for physical separation and attendant loss of textural information. In recent years, instrumental and technical advances have led to improvements in precision to the point where reproducibility is often better than 1‰ and within 1–5 times that of conventional analyses for H, C, S, B, and O isotopes (see Table 1). These precision levels allow the ion microprobe to be usefully applied to the study of a variety of geological processes, as well as opening new areas of research in cosmochemistry.

In spite of these advances, there are still limitations that restrict the use of the ion microprobe in geolog-

* Corresponding author.

[1] Currently at: Isotopic Analytical Services Ltd., Aberdeen Science Park, Aberdeen AB22 8GW, Scotland, UK.

[2] Currently at: Dept. of Geology, Univ. of Puerto Rico at Mayagüez, P.O. Box 9017, Mayagüez, PR 00681-9017.

Dedicated to the memory of Al Nier.

PII S1387-3806(98)14088-5

Table 1
Typical values for isotope analysis by conventional (gas source) techniques and SIMS

					SIMS		
	Phase	Conventional precision (1σ)	Sample size	Ref.	Precision (1σ)	Sample size	Ref.
$\delta^{18}O$	Silicates, oxides	Ni-rod bomb ±0.2‰ laser ±0.1‰	10–20 mg 0.5 mg	[56] [57]	±0.6–1.0‰	5–10 ng	[4,13,15]
$\delta^{18}O$, $\delta^{13}C$	Carbonates	Phosphoric ±0.03–0.1‰	10 μg	[58,59]	±0.6–2.0‰	5–30 ng	[15,30,48,49]
$\delta^{13}C$	Graphite, diamond	Combustion ±0.03‰	1 μg	[60]	±0.5–1.0‰	5–10 ng	[65,66]
$\delta^{34}S$	Sulfides	Combustion ±0.1‰ laser ±0.2‰	1 mg 0.1 mg	[61] [62]	±0.25–1.0‰	0.5–5 ng	[12,16,22]
δD	Silicates, oxides	±1–2‰	50–100 mg	[63,64]	±3–10‰	3–20 ng	[6,10,11]

ical studies. Isotopic fractionation occurs at a variety of stages during SIMS analysis, including sputtering, ionization, extraction, transmission of the secondary ions through the mass spectrometer, and secondary ion detection. However, these conditions can be held constant by the operator. More problematic is the "matrix effect," wherein the chemical composition of the analyte affects measured isotope ratios. The combination of these effects, which almost always favor the light isotope and can result in fractionations of a few to 100's of per mil from the "true" value, is termed the instrumental mass bias. To obtain accurate isotope ratio measurements the mass bias needs to be adequately quantified and controlled for the mineral phase being analyzed. The correction of mass bias is straightforward for isochemical phases when matrix-matched standards are available. However, most minerals are complex solid solutions, requiring either an extensive suite of standards (that can be time consuming, expensive, and difficult to develop) or predictive models that relate mass bias to mineral composition.

In this paper we develop further themes outlined in a talk given at the 3rd Nier Conference, which reviewed the factors that influence instrumental mass bias during SIMS analysis of light stable isotope ratios in minerals. Although this article focuses primarily on compositional matrix effects, the influence of instrumental parameters on sulfur isotope ratio measurements is also explored. In addition, recent empirical models that relate mass bias to matrix composition are summarized.

2. Experimental techniques

The data reported in this study were obtained by using a modified Cameca 4f ion microprobe equipped with a normal incident electron gun, Cs^+ microbeam and duoplasmatron ($^{16}O^-$ and $^{16}O_2^+$) primary ion sources, and an air lock that allows two samples to be kept under vacuum. The instrument has been modified to allow the secondary ion accelerating voltage to be continuously varied between 0 and 5000 V. An ETP 133H electron multiplier was used to detect the ion signals. The standard Cameca ion counting system has been replaced by a Pulse-Count Technology system resulting in a lower system deadtime (between 13.5 and 17.0 ns for the measurements described in this paper).

A variety of experimental conditions, summarized below, were used for the measurement of light stable isotope ratios. The main factor governing the choice of instrumental parameters is whether the mineral phase to be analyzed is an electrical insulator or conductor. If an insulating sample is Au coated, the use of an O^- primary ion beam and positive secondary ions results in minimal sample charging. These are the conditions most commonly used for trace element analysis and B and H isotope measurements [e.g. 8–11]. For electronegative elements (O, C, S, and, to a lesser extent, H), ion yields (and potentially precision) are strongly enhanced by sputtering with a Cs^+ primary ion beam and analysis of negative secondary ions. However, these analytical conditions

lead to severe charging of insulating materials, including most geological materials.

An additional problem that must be overcome is that of molecular interferences, particularly hydrides of the light mass isotope. Two different analytical methods that use different populations of secondary ions have been developed. High mass resolution utilizes secondary ions with low initial kinetic energies (~0 eV), whereas extreme energy filtering uses secondary ions with high initial kinetic energies, typically >300 eV. For high mass resolution, the secondary ion beam is collimated by using the entrance slit, field aperture, and energy slits, and the exit slit is closed to provide sufficient mass resolution [e.g. 12]. For low energy secondary ions, mass bias is very sensitive to the energy of the ion, and thus, high mass resolution analyses are susceptible to problems arising from sample charging [e.g. 13]. Extreme energy filtering utilizes the fact that the energy distribution of molecular ions is much narrower than that of atomic ions, so the proportion of hydride species relative to atomic species decreases with increasing secondary ion kinetic energy, and hydride abundances are insignificant at energies >300 eV [11,12]. The use of extreme energy filtering (typically by offsetting the sample voltage 325–350 V relative to the acceptance energy of the mass spectrometer) allows the mass spectrometer to be operated at low mass resolution, greatly simplifying instrument tuning [e.g. 13]. For voltage offsets >300 V, mass bias is relatively insensitive to slight fluctuations in ion energy. Therefore, stable analytical conditions can be achieved for the analysis of insulators with the Cameca 3f and 4f instruments by using an electron gun to compensate for sample charging [e.g. 13,15].

Most sulfide minerals are conductors and thus provide the opportunity to investigate the influence of a variety of instrument parameters on mass bias. A series of experiments was performed by using $^{16}O^-$, $^{16}O_2^+$ (both accelerated at 12.5 keV) and $^{133}Cs^+$ (10 keV) primary ions. Analyses were performed by using both positive and negative secondary ions with a mass resolution in excess of 4000 m/Δm to resolve isobaric interferences, mainly sulfur hydrides, O_2^+, O_2^-, and $^{64}Zn^{2+}$ species [1,16]. The magnet was cycled between the ^{32}S and ^{34}S peaks, counting for 1 s on ^{32}S, 5 s on ^{34}S, and employing a 1 s magnet settle time. Experiments that use the Cs^+ primary ion beam and negative secondary ions collected at low mass resolution with a voltage offset of 350 V (extreme energy filtering) were undertaken to explore the effects of varying secondary ion energy [16,17]. Counting times were identical to those of the high mass resolution analyses, but the magnet settling time was reduced to 0.3 s. For all analyses, the energy slits were set at a bandpass of ±20 V. Depending on the count rate, from 70 to 150 individual ratios were measured for each analysis. Total analysis time ranged from 15 to 30 min.

Oxygen and carbon isotope analyses were undertaken by using extreme energy filtering of negative secondary ions, offset voltages between 320 and 350 V, and the normal incident electron gun for charge compensation [15]. Samples were sputtered by using a mass-filtered Cs^+ primary ion beam accelerated to 10 keV. Primary beam currents ranged between 3 and 10 nA with a ~15–35 μm diameter spot size. For oxygen isotope measurements, a total of 100–200 ratios were measured for each analysis, with ^{16}O counted for 1 s, ^{18}O counted for 5 s, and a 0.3 s magnet settle time. The initial count rate on ^{16}O was adjusted to 1.4×10^6 cps by varying the primary beam current. The theoretical counting statistical precision for these analyses, based on the total ^{18}O counts, was ±0.7–1.1‰ (1σ) depending on the number of ratios measured. The internal precision of each individual analysis, assessed by the standard error of the individual ratios comprising the analysis, was typically within 0.2‰ of the theoretical limit. Total analysis time was ~15–25 minutes. For carbon isotope measurements, 100–350 ratios were measured for each analysis, with 1 s and 5 s count times for ^{12}C and ^{13}C, respectively. Total analysis time was ~15–60 min. Internal precision was between 1.5 and 3‰.

A number of minerals of varying chemical composition were used in this study. Major element compositions were determined and mineral homogeneity evaluated by using a Cameca SX50 electron microprobe at the University of Tennessee–Knoxville

Table 2
Composition of sulfide minerals [Py = pyrite, Po = pyrrhotite, Pnt = pentlandite, Sph = sphalerite, Cpy = chalcopyrite, Tr = troilite. All mineral analyses (elemental and isotopic) from [67], except for CDT]

wt ‰	Balmat Py	Anderson Po	Norilsk Pnt	Balmat Sph	Chisel Sph	Trout Lk Cpy	Norilsk Cpy	CDT Tr[a]
Fe	44.54	58.25	30.28	5.90	7.86	30.01	29.98	65.53
Cu	0.04	0.03	0.41	0.00	0.00	35.67	34.63	0.00
Zn	0.01	0.00	0.02	62.56	60.15	0.12	0.00	0.00
Ni	...	...	35.17	...	...	...	0.05	0.00
Co	0.00	0.00	0.25	0.00	0.00	0.00	0.00	0.00
S	52.41	38.47	33.90	32.75	33.15	34.62	34.98	36.47
Sum	97.00	96.75	100.03	101.18	101.16	100.42	99.63	100.00
$\delta^{34}S_{CDT}$‰	15.1	1.4	7.9	14.3	1.5	0.3	8.0	0.0

[a] Composition calculated assuming ideal formula.

(see Tables 2, 3, and 4). Between 10 and 50 major element analyses were determined for each mineral phase. Sulfur, oxygen, and carbon isotope ratios were measured in a number of laboratories by using conventional gas-source mass spectrometry. In addition, several minerals of each type were analyzed in at least two laboratories. For a number of samples, the stable isotope ratios were analyzed in multiple chips to check for homogeneity on the macroscale. However, the only way to evaluate micron-scale homogeneity is by examining the reproducibility of multiple ion microprobe analyses. Precision and reproducibility of conventional analyses is typically ± 0.2–0.3‰ for $\delta^{18}O$, $\delta^{13}C$, and $\delta^{34}S$ (e.g. Table 1).

All samples were mounted in epoxy resin in holes drilled in 25 mm diameter aluminum blocks suitable for mounting in a standard Cameca sample holder. These sample blocks were polished by using a final grit size of 1 μm or finer. Typically 12 to 21 minerals were mounted in each sample block, with at least one "reference" mineral in each block to provide a means of monitoring mass bias differences between blocks. Following ultrasonic cleaning in distilled water and methanol, samples were gold coated to ensure surface conductivity.

3. Data presentation

All data are presented by using standard δ-notation relative to the appropriate international standards: Canyon Diablo Troilite (CDT) for $^{34}S/^{32}S$, Standard Mean Ocean Water (V-SMOW) for $^{18}O/^{16}O$, and Peedee Belemnite (PDB) for $^{13}C/^{12}C$. The equation for calculating δ values (by using $\delta^{34}S$ as an example) is as follows:

$$\delta^{34}S = [[(^{34}S/^{32}S)_{sample}/(^{34}S/^{32}S)_{CDT}] - 1] \times 1000 \quad (1)$$

Isotope ratios measured by SIMS were compared to accepted ratios (calculated from δ values determined by gas source mass spectrometry) for each mineral by using Eq. (2) (again by using sulfur as an example):

$$(^{34}S/^{32}S)_{sample} = [(\delta^{34}S_{sample}/1000) + 1] \times (^{34}S/^{32}S)_{CDT} \quad (2)$$

where the $^{34}S/^{32}S$ ratio of CDT is defined as $4.500\,45 \times 10^{-2}$ [18]. The $^{18}O/^{16}O$ ratio of V-SMOW is defined as 2.0052×10^{-3} [19], and the $^{13}C/^{12}C$ ratio of V-PDB defined as $1.119\,49 \times 10^{-2}$ [20,21]. These data can be used to calculate the isotope mass fractionation that occurs during SIMS analysis by using Eq. (3):

$$\beta_{inst} = (^{34}S/^{32}S)_{SIMS}/(^{34}S/^{32}S)_{gas\ source} \quad (3)$$

where $^{34}S/^{32}S_{SIMS}$ is the ratio measured by using SIMS and $^{34}S/^{32}S_{gas\ source}$ the accepted ratio measured by using gas source mass spectrometry. For simplicity, β_{inst} can be converted into per mil (‰) notation by using Eq. (4):

Table 3
Silicate and oxide mineral major element and oxygen isotope ratios

Garnets (Gnt)

	437	JE3	J546	J147	JH1	Gspd	PyQ	438	Brk	Mel	May
SiO_2	40.75	40.21	39.70	40.88	41.12	39.54	43.63	38.99	35.79	35.22	39.06
TiO_2	0.06	0.12	0.09	0.05	0.01	0.15	0.01	0.10	0.04	0.04	0.06
Al_2O_3	22.89	23.00	22.81	19.26	22.39	22.57	25.30	22.58	21.21	2.04	22.17
Cr_2O_3	1.07	0.16	0.11	5.63	2.17	0.04	0.01	0.06	0.02	0.00	0.00
MgO	19.60	17.27	13.17	20.53	20.60	7.66	29.80	11.80	4.63	0.02	10.81
CaO	4.19	3.79	11.07	5.46	4.61	18.07	0.09	8.59	0.63	32.65	3.33
MnO	0.46	0.36	0.34	0.32	0.42	0.27	0.01	0.40	2.32	0.18	16.19
FeT	10.49	14.36	11.65	7.27	8.45	11.64	1.49	16.73	33.92	26.53	7.62
FeO	8.17	12.26	9.73	5.21	6.33	10.39	0.00	14.44	31.68	0.00	5.62
Fe_2O_3	2.58	2.34	2.14	2.30	2.36	1.40	1.65	2.54	2.50	29.67	2.23
Sum	99.77	99.51	99.16	99.63	100.01	100.08	100.62	99.51	98.81	99.82	99.47
$\delta^{18}O_{SMOW}$	5.0	7.0	2.8	5.3	5.4	7.5	5.5	3.0	6.7	8.3	12.6

	GM	AZ	Mex	JL1	G143	1146	GrA	Sps	And	Mal
SiO_2	38.13	39.99	38.31	41.29	39.39	40.57	38.07	34.84	34.59	37.06
TiO_2	0.11	0.22	0.59	0.47	0.23	0.10	0.46	0.08	0.01	1.10
Al_2O_3	22.32	22.28	19.82	20.85	22.72	23.15	22.16	20.48	0.13	12.27
Cr_2O_3	0.01	1.21	0.01	2.92	0.14	0.25	0.01	0.02	0.00	0.03
MgO	10.52	18.04	0.68	21.46	14.03	17.07	0.01	0.00	0.05	0.50
CaO	5.84	4.91	35.60	4.60	4.45	7.07	35.40	0.11	33.85	34.82
MnO	0.51	0.48	0.41	0.30	0.72	0.34	0.39	39.36	0.23	0.30
FeT	21.62	11.90	2.78	7.70	17.91	11.10	1.51	2.81	27.58	12.29
FeO	19.21	9.19	0.00	5.38	15.99	8.95	0.52	1.92	0.00	0.00
Fe_2O_3	2.68	3.01	3.09	2.59	2.13	2.40	1.11	0.99	30.70	13.67
Sum	99.27	99.34	98.51	99.85	99.81	99.89	98.12	97.80	99.56	99.75
$\delta^{18}O_{SMOW}$	5.9	4.2	10.6	5.4	7.3	5.3	3.5	5.4	−3.6	9.3

Olivines (Oliv) + monticellite (Mont)

	J147	SL18	All	CM	Ami	1888	ESt	Spw	Mont
SiO_2	40.52	40.39	42.75	42.13	39.91	39.73	38.51	38.86	37.33
MgO	49.76	48.05	57.35	55.67	53.42	45.80	41.76	43.57	22.49
CaO	0.00	0.00	0.00	0.33	0.00	0.00	0.00	0.00	34.77
MnO	0.11	0.12	0.00	0.04	0.15	0.13	0.17	0.31	0.43
FeO	8.89	11.05	0.00	1.91	5.21	13.85	19.11	16.97	3.94
NiO	0.39	0.38	0.00	0.07	0.00	0.30	0.00	0.00	0.00
Sum	99.28	99.61	100.10	100.08	98.69	99.51	99.55	99.71	98.91
$\delta^{18}O_{SMOW}$	5.2	5.2	7.2	7.8	12.3	5.1	−2.9	2.9	21.9

Feldspar (Fsp)

	Am	Ont	SP	MAn	Shrp	JAn	OLa	MBy	SHR6
SiO_2	68.11	64.10	64.19	55.89	53.20	43.17	49.44	52.33	64.71
Al_2O_3	19.68	18.44	18.55	27.62	29.22	35.36	31.25	26.46	18.58
CaO	0.12	0.00	0.01	9.71	11.36	19.01	14.29	12.01	0.08
FeO	0.02	0.03	0.01	0.12	0.13	0.50	0.37	0.34	0.08
Na_2O	11.50	0.69	0.67	5.74	4.82	0.49	3.21	4.33	2.43
K_2O	0.14	16.08	16.16	0.33	0.20	0.01	0.05	0.38	13.38
Sum	99.57	99.34	99.59	99.41	98.93	98.54	98.61	95.85	99.26
$\delta^{18}O_{SMOW}$	10.6	10.3	10	9.6	8.4	5.6	5.0	5.9	

continued

Table 3
(continued)

(Px = pyroxene, Qtz = quartz, Kyan = kyanite, Rt = rutile, Mt = magnetite)										
	CrA	183	Casc	Bz	BOG	Carr	N-28	Ky	SHR4	LP204
	Px	Px	Px	Qtz[a]	Qtz[a]	Qtz[a]	Qtz[a]	Kyan[a]	Rt[a]	Mt
SiO_2	50.12	52.62	52.49	100.00	100.00	100.00	100.00	35.80		0.00
TiO_2	0.48	0.63	0.11						100.00	0.16
Al_2O_3	7.49	5.22	2.05					64.20		1.66
Cr_2O_3	0.89	0.29	0.02							0.00
MgO	17.26	18.24	16.72							1.05
CaO	17.41	14.74	25.83							0.00
MnO	0.13	0.13	0.08							3.43
FeO	4.73	5.79	2.26							93.00
Na_2O	0.84	1.68	0.01							0.00
Sum	99.35	99.34	99.57							99.3
$\delta^{18}O_{SMOW}$	4.9	6.2	20.9	21.5	12.3	31.3	9.6	8.0	6.9	8.6

[a] Composition calculated by using idealized formula.

$$\delta^{34}S_{bias} = [(^{34}S/^{32}S)_{SIMS}/(^{34}S/^{32}S)_{gas\ source} - 1] \times 1000 = (\beta_{inst} - 1) \times 1000 \quad (4)$$

For all analyses in this paper, the light isotope is enriched during SIMS analysis, so $\delta^{34}S_{bias}$ values are always negative. This makes terminology somewhat confusing. In this article, changes in mass bias are discussed in terms of absolute values. Therefore, decreasing $\delta^{34}S_{bias}$ *values* (larger negative numbers) indicate that mass bias is larger. Conversely, decreas-

Table 4
Carbonate standard compositions and measured $\delta^{13}C_{bias}$ and $\delta^{18}O_{bias}$ values [Chemical Comp. = atomic proportion of elements in each standard, determined by electron probe by using WDS. $\delta^{13}C_{PDB}$ = accepted carbon isotope value of mineral relative to PDB standard (see text). $\delta^{18}O_{SMOW}$ = accepted oxygen isotope value of the mineral relative to the SMOW standard. The conventionally measured (phosphoric acid liberated) $\delta^{18}O$ values have been corrected to the value expected for total oxygen in the sample. $\delta^{13}C_{bias}$, $\delta^{18}O_{bias}$ = SIMS instrumental mass bias (see text). $\delta^{13}C$ error, $\delta^{18}O$ error = 1σ error on repeated analyses of each mineral (n = 3–6)]

Sample	Chemical comp.	$\delta^{13}C_{PDB}$ (‰)	$\delta^{18}O_{SMOW}$ (‰)	$\delta^{13}C_{bias}$ (‰)	$\delta^{13}C$ 1σ error	$\delta^{18}O_{bias}$ (‰)	$\delta^{18}O$ 1σ error
Carr Cc	$Ca_{1.00}CO_3$	2.1	18.5	−68.7	1.8	−68.1	0.3
UT Cc	$Ca_{1.00}CO_3$	−10.6	11.0	−70.5	1	−67.6	0.3
DRC Arag	$Ca_{1.00}CO_3$	2.6	11.5	−67.0	1.9	−67.4	0.8
With-1	$Ba_{0.975}\ Sr_{0.025}CO_3$	−16.4	9.1	−41.6	2.1	−12.6	1.4
Stront-1	$Sr_{0.789}\ Ca_{0.209}Ba_{0.002}CO_3$	−8.6	11.8	−54.9	1.7	−35.2	1.4
Cerr-1	$Pb_{0.998}Sr_{0.002}CO_3$	−11.5	3.0	−52.1	0.3	−22.5	1.5
LRR Sid	$Fe_{0.952}Mn_{0.044}Mg_{0.003}Ca_{0.001}CO_3$	−8.3	−1.5	−46.5	2.1	−29.7	0.1
DRC Sid	$Fe_{0.635}Mn_{0.008}Mg_{0.350}Ca_{0.007}CO_3$	−5	0.4	−50.0	1.5	−44.1	0.1
ZS Sid	$Fe_{0.801}Mn_{0.143}Mg_{0.049}Ca_{0.007}CO_3$	−11	7.8	−46.1	1.6	−30.6	1.0
DRC Rhod	$Mn_{0.988}Mg_{0.002}Ca_{0.010}CO_3$	−5.7	−3.0	−49.4	0.7	−32.6	0.9
ZS Rhod	$Mn_{0.922}Mg_{0.009}Ca_{0.069}CO_3$	−7.5	7.7	−48.8	2.9	−38.8	0.4
ZS Smith	$Zn_{0.956}Fe_{0.002}Mn_{0.003}Mg_{0.020}Ca_{0.020}CO_3$	−11.1	15.1	−66.7	1.8	−45.4	0.7
LRR Smith	$Zn_{0.940}Cu_{0.060}CO_3$	0.6	15.6	−64.0	1.1	−45.7	0.4
DRC Magn	$Fe_{0.002}Mn_{0.001}Mg_{0.993}Ca_{0.005}CO_3$	2.8	8.3	−77.5	1.4	−99.6	1.1
DM Dol	$Fe_{0.021}Mn_{0.002}Mg_{0.438}Ca_{0.539}CO_3$	−2.6	−0.9	−72.8	1.6	−76.3	0.6
DM C2	$Mg_{0.032}Ca_{0.968}CO_3$	1.7	8.1	−70.3	2.3	−69.6	0.6
DRC Dol	$Fe_{0.001}Mg_{0.462}Ca_{0.538}CO_3$	0.9	1.8	−73.3	2.1	−75.3	0.2
LR FeDol	$Fe_{0.088}Mn_{0.095}Mg_{0.287}Ca_{0.530}CO_3$	−8.1	2.6	−60.4	2.6	−58.8	0.7
LR NorDol	$Fe_{0.077}Mn_{0.002}Mg_{0.373}Ca_{0.548}CO_3$	−8.3	2.3	−64.1	1.1	−64.8	0.3
DRC Ank	$Fe_{0.159}Mn_{0.006}Mg_{0.289}Ca_{0.546}CO_3$	−3.6	0.7	−60.5	1.3	−56.6	0.4

ing mass bias corresponds with increasing $\delta^{34}S_{bias}$ values (less negative numbers).

4. Results

The results of over 1500 ion microprobe oxygen, carbon, and sulfur isotope ratio measurements are summarized in this article. Additional information is available from the senior author on request.

4.1. Sulfur isotopes

The results obtained by using negative and positive secondary ions are summarized in Tables 5 and 6, respectively. The bulk of the data was collected by using negative secondary ions, as (1) superior precision is obtained and (2) these data can be more directly compared to the mass bias behavior of oxygen and carbon. More limited data was collected by using positive secondary ions, as there are several sources of literature values for sulfur mass bias obtained by using positive secondary ions and oxygen primary ion beams [22–25]. The cumulative data set allows consideration of mass bias effects arising from use of various primary ions and secondary ion polarity and energy. Mass bias has also been demonstrated to depend on primary ion energy [26], but these effects were not directly investigated in this study. To minimize errors associated with session-to-session calibration of the instrument, all analyses associated with a particular experiment (e.g., matrix effects with a Cs^+ primary beam and negative secondary ions) were run in the same analytical session. No intrasession drift correction was necessary, as isotope ratios measured on a particular standard remained constant during individual, continuous analytical sessions, even for sessions that exceeded 100 h duration.

4.1.1. Effect of changes in offset voltage

A series of experiments were run in which the sample accelerating voltage was varied relative to the acceptance energy of the mass spectrometer (4500 ± 20 V) to examine the effect of the secondary ion kinetic energy on mass bias (Figs. 1 and 2). For positive secondary ions, the general relationship between secondary ion energy and mass bias is similar for both Cs^+ and O_2^+ primary beams; there is insufficient data using an O^- primary beam to judge any trend. Mass bias decreased by 10 to 20‰ as the offset voltage was increased from 0 to 20–40 V, behavior similar to that documented by Gnaser and Hutcheon [27] for other light elements. Following this initial decrease, mass bias rapidly increased ($\delta^{34}S_{bias}$ values become more negative) with increasing offset voltage, with gradients of ~0.3‰/eV.

For negative secondary ions, the change in mass bias as a function of initial kinetic energy varies with the type of primary ion beam (Fig. 2). For analyses that use a Cs^+ primary ion beam, mass bias increased with increasing offset voltage. The magnitude of the increase was not nearly as great as for positive secondary ions (~0.06‰/eV); the gradient decreased with increasing secondary ion energy. This is similar to mass bias behavior observed when analyzing negative oxygen secondary ions sputtered by a Cs^+ primary beam [13]. The behavior of negative secondary ions sputtered by using oxygen primary beams is different (Fig. 2). For sputtering with both O^- and O_2^+, $\delta^{34}S_{bias}$ decreased (by ~25‰) as the offset voltage was increased from 0 to 100 V. For secondary ions with initial kinetic energy greater than 100 eV, mass bias remained relatively constant (decreasing only a few ‰) with further increases in offset voltage.

Although variations in mass bias due to instrument tuning make it difficult to compare the magnitude of mass bias under different analytical conditions, some generalities are clear as illustrated by using the mineral pyrrhotite (Fig. 3). Low-energy, negative secondary ions sputtered by a Cs^+ primary beam have the smallest mass bias (−10 to −30‰ $\delta^{34}S_{bias}$ values). In contrast, low-energy, negative secondary ions sputtered by oxygen primary ion beams have the largest mass biases (−80 to −120‰). Low-energy, positive secondary ions have intermediate $\delta^{34}S_{bias}$ values (−60 to −30‰) for all three primary ion beams that were employed. Compared to positive ions, mass bias measured for negative secondary ions is much less sensitive to variations in secondary ion energy.

Table 5
Instrumental mass bias measured on sulfide minerals by using negative secondary ions [$^{34}S/^{32}S$: Measured $^{34}S/^{32}S$ ratio, IP‰: average internal precision of the individual analyses for each mineral under those conditions, σ‰: error (1 standard deviation) of the instrumental mass bias, determined by the reproducibility of n analyses]

Phase	Cpy	Cpy	Pnt	Pnt	Po	Py	Sph	Tr	Cpy	Po	Py	Py	Py	Sph	Sph
Standard	Trout Lk	Norilsk	Kambald	Norilsk	Anderson	Balmat	Balmat	CDT	OPM721	Enonko	Calum	123	AJH 1	AJH	Chisel
"True" $^{34}S/^{32}S \times 100$	4.5018	4.5362	4.5104	4.5362	4.5068	4.5684	4.565	4.50045	4.5107	4.5045	4.5167	4.5068	4.4797	4.4347	4.5071
3/14/95, Cs^+ primary beam, 350 V offset															
# Anal	426.6	4	4	4	5	18	5		4	5	5	5	6	5	5
$^{34}S/^{32}S \times 100$	4.2843	4.3198	4.2829	4.2981	4.2737	4.3506	4.3701		4.2975	4.2750	4.3063	4.2889	4.2653	4.2283	4.3015
IP‰	0.24	0.23	0.22	0.22	0.21	0.22	0.25		0.22	0.20	0.23	0.22	0.22	0.27	0.27
$\delta^{34}S_{bias}$‰	−48.3	−47.7	−50.4	−52.5	−51.7	−47.7	−42.7		−47.3	−50.9	−46.6	−48.4	−47.8	−46.6	−45.6
σ‰	0.24	0.19	0.24	0.35	0.22	0.36	0.60		0.36	0.30	0.70	1.48	0.44	1.53	1.16
3/20/95, Cs^- primary beam, 0 V offset															
# Anal	3	3	4	3	3	4									
$^{34}S/^{32}S \times 100$	4.3820	4.4142	4.3900	4.4021	4.3767	4.4464									
IP‰	0.24	0.23	0.52	0.25	0.38	0.32									
$\delta^{34}S_{bias}$‰	−26.6	−26.9	−26.7	−29.6	−28.9	−26.7									
σ‰	0.06	0.66	0.74	0.26	1.18	0.51									
7/6/95, O^- primary beam, 0 V offset															
# Anal					4	8		4							
$^{34}S/^{32}S \times 100$					4.0503	4.1079		4.0502							
IP‰					0.47	0.48		0.47							
$\delta^{34}S_{bias}$‰					−101.3	−100.8		−100.0							
σ‰					0.84	0.62		0.84							
8/29/95, O^- primary beam, 0 V offset															
# Anal	4		4		4	5	3	3							
$^{34}S/^{32}S \times 100$	4.0295		4.1217		4.0483	4.0974	4.1818	4.0501							
IP‰	0.40		0.32		0.33	0.32	0.41	0.27							
$\delta^{34}S_{bias}$‰	−104.9		−90.1		−101.7	−103.7	−84.0	−100.1							
σ‰	0.15		0.54		0.34	0.82	0.85	0.80							
7/7/95, O_2^+ primary beam, 0 V offset															
# Anal		4			3	7		4							
$^{34}S/^{32}S \times 100$		4.0921			4.036	4.0934		4.0399							
IP‰		0.49			0.44	0.35		0.31							
$\delta^{34}S_{bias}$‰		−97.6			−104.5	−104.0		−102.3							
σ‰		1.24			0.37	0.39		0.53							
8/28/95, O_2^+ primary beam, 0 V offset															
# Anal	4			4	4	4		4							
$^{34}S/^{32}S \times 100$	4.0921			4.1361	4.0708	4.1247		4.0583							
IP‰	0.37			0.44	0.31	0.45		0.32							
$\delta^{34}S_{bias}$‰	−91.0			−88.2	−96.8	−97.1		−98.3							
σ‰	0.96			1.14	0.28	1.00		1.14							

Table 6
Instrumental mass bias measured on sulfide minerals by using positive secondary ions [$^{34}S/^{32}S$: Measured $^{34}S/^{32}S$ ratio, IP‰: average internal precision of the individual analyses for each mineral under those conditions, σ‰: error (1 standard deviation) of the instrumental mass bias, determined by the reproducibility of n analyses]

Phase	Cpy	Pnt	Po	Py
Standard	Trout Lk	Kambald	Anderson	Balmat
"True" $^{34}S/^{32}S \times 100$	4.5018	4.5104	4.5068	4.5684
3/21/95, Cs^+ primary beam, 0 V offset				
# Anal	2	2	1	
$^{34}S/^{32}S \times 100$	4.2369	4.2829	4.2513	
IP‰	0.49	1.08	0.69	
$\delta^{34}S_{bias}$‰	−58.9	−58.3	−56.7	
σ‰	1.5	1.2	n.a.	
4/6/95, O^- primary beam, 0 V offset				
# Anal	2		3	3
$^{34}S/^{32}S \times 100$	4.382		4.3137	4.3817
IP‰	1.28		1.15	1.05
$\delta^{34}S_{bias}$‰	−48		−42.9	−40.9
σ‰	0.8		1	1.3
3/28/95, O_2^+ primary beam, 0 V offset				
# Anal	5		4	3
$^{34}S/^{32}S \times 100$	4.3933		4.3964	4.4464
IP‰	0.79		0.81	0.78
$\delta^{34}S_{bias}$‰	−24.1		−24.5	−26.7
σ‰	0.5		2.7	1.4

4.1.2. Sulfur ion yields

A Cs^+ primary ion beam enhances secondary ion yields for both positive and negative ions (Fig. 4), and for any primary beam, ion yields are typically greater

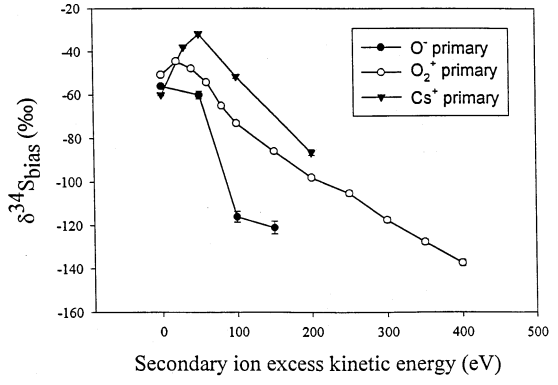

Fig. 1. Pyrite $\delta^{34}S_{bias}$ values as a function of secondary ion energy for positive secondary ions. Most 1σ error bars are smaller than symbols.

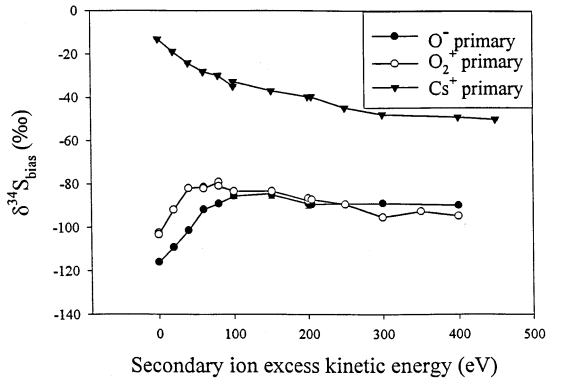

Fig. 2. Pyrite $\delta^{34}S_{bias}$ values as a function of secondary ion energy for negative secondary ions. Most 1σ error bars are smaller than the symbols.

for negative secondary ions. Change in ion yield as a function of offset voltage is similar under all analytical conditions, decreasing by 2–3 orders of magnitude with increases in offset voltage from 0 to 100–200 V. However, the gradient of this decrease is steeper for positive secondary ions and, as discussed below, correlates with increased sensitivity of mass bias as a function of mineral chemistry for positive secondary ions.

In general, relative sulfur ion yields of the different minerals are similar irrespective of instrumental conditions (Fig. 5). Pentlandite and pyrrhotite typically

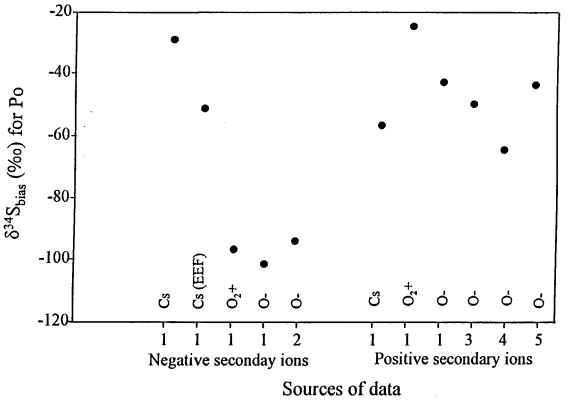

Fig. 3. Summary of pyrrhotite $\delta^{34}S_{bias}$ values as a function of primary ion beam and secondary ion polarity. Data sources: 1—this study; 2—[25]; 3—[24]; 4—[23]; 5—[22]. 1–4 were obtained by using Cameca 3f or 4f instruments, 5 by using SHRIMP. 1‰ error bars are smaller than the symbols.

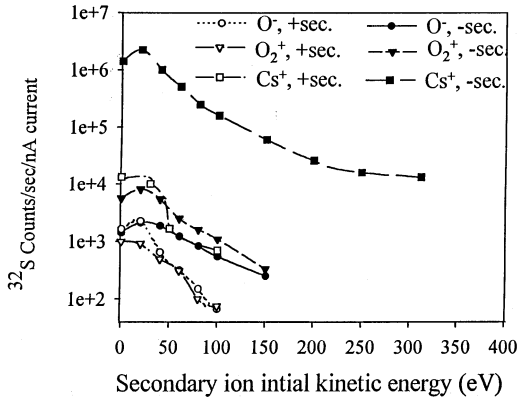

Fig. 4. Pyrite ^{32}S ion yield as a function of primary ion beam and secondary ion polarity.

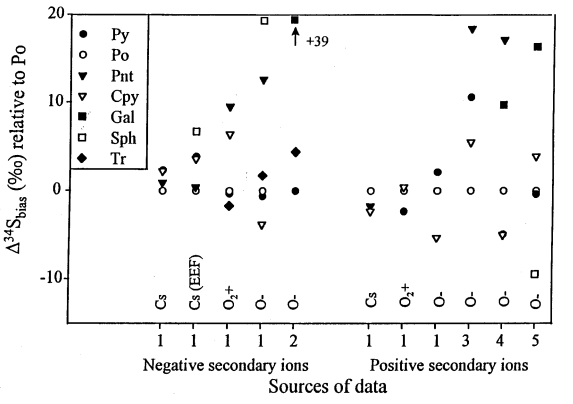

Fig. 6. Summary of $\delta^{34}S_{bias}$ values for a variety of minerals under different instrumental conditions. Mass bias values have been normalized to that measured on pyrrhotite (Po). Data sources: 1—this study; 2—[25]; 3—[24]; 4—[23]; 5—[22]. All data obtained by using low energy secondary ions with the exception of Cs (EEF). Abbreviations after Fig. 5; Gal-galena.

have the lowest ion yields, and chalcopyrite the highest. This range in relative ion yields decreases when high-energy secondary ions are analyzed, behavior that has been observed for other elements [e.g., 28]. There is no obvious relationship between ion yield and the atomic proportion of sulfur in the different minerals.

4.1.3. Sulfur isotope mass bias

The relationships between matrix composition, instrumental conditions, and mass bias from both our work and published values are summarized in Tables 5 and 6 and Fig. 6. The following general observations are based on results for chalcopyrite, pyrite, pentlandite, and pyrrhotite.

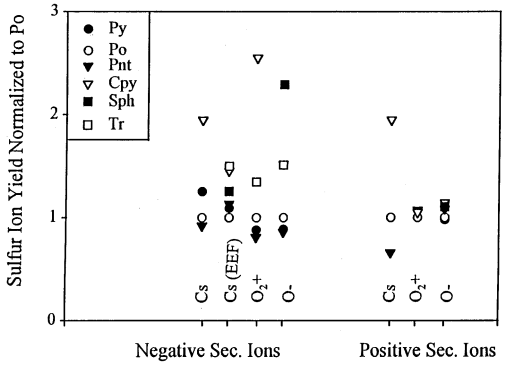

Fig. 5. ^{32}S ion yield from different minerals as a function of primary ion beam and secondary ion polarity. Ion yields are normalized to that of pyrrhotite (Po). All data obtained by using low energy ions with the exception of Cs (EEF). Py—pyrite; Po—pyrrhotite; Pnt—pentlandite; Cpy—chalcopyrite; Sph—sphalerite; Tr—troilite (Table 2).

(1) When analyzing negative secondary ions, the range in mass bias is much smaller when using a Cs^+ primary ion beam compared to either polarity of oxygen primary beam. For pyrrhotite, pyrite, chalcopyrite, and pentlandite, the range in $\delta^{34}S_{bias}$ values is only 3‰ when using a Cs^+ primary ion beam (for low-energy ions), 9‰ when using an O_2^+ primary beam, and 15‰ for an O^- primary beam (Fig. 6).

(2) When using a Cs^+ primary ion beam, differences in mass bias are slightly larger for high-energy secondary ions when compared to low-energy secondary ions. For the same set of minerals, the variation in mass bias increases from 3‰ at 0 V offset to 5‰ for a 350 V offset. For both low and high-energy secondary ions, the relative fractionation between the different minerals is similar, Po < Pt < Cpy ≤ Py (Fig. 6).

(3) For both positive and negative secondary ions, the use of an O^- primary ion beam appears to result in the largest range in mass bias between different minerals (Fig. 6).

(4) Comparison of results from different laboratories shows that relative differences in mass bias measured by using nominally similar conditions (e.g.,

O^- primary ion beam; low energy positively charged secondary ions) vary by up to 10‰ (Fig. 6).

4.2. Oxygen and carbon isotopes

The results of extreme energy filtering analyses of oxygen isotopes in silicate and oxide minerals, and oxygen and carbon isotopes in carbonates, are summarized in Tables 7 and 4, respectively. In general, as would be expected for homogeneous materials, reproducibility as assessed by the standard deviation of repeat analyses on any given mineral is similar to or better than the internal precision of individual analyses. Within individual analytical sessions (from 8 to over 100 h) we did not observe any drift in mass bias as monitored by periodic analysis of a particular standard. The average mass bias that we measured on any given mineral is similar to those measured by other laboratories utilizing extreme energy filtering [13,29].

4.2.1. Long-term reproducibility

The absolute mass bias measured on quartz (SiO_2) during analytical sessions over a three-year period has varied between −65‰ and −85‰, with most values falling between −69 and −75‰ (Fig. 7). The session-to-session variation is partially due to differences in instrumental parameters such as mass spectrometer tuning and electron gun alignment. However, the dominant cause is change in electron multiplier response with time. The largest deviations from the median quartz mass bias value can be correlated with changes in conversion efficiency of the electron multiplier. Session-to-session variation can be minimized by checking the relative Faraday cup/electron multiplier (FC/EM) response and increasing the electron multiplier high voltage to maintain a constant FC/EM ratio.

Session-to-session changes in mass bias require the instrument to be calibrated every analytical session. This is simple for isochemical materials, as an appropriate standard can be analyzed and used to calibrate the mass bias. For chemically complex systems, it is not feasible to calibrate matrix-mass bias relations involving multiple standards every session. However, although absolute values of mass bias may vary significantly, the relative difference in mass bias between different minerals is similar from session to session. Isotope ratios measured on different minerals in different sessions can be normalized by using ratios measured on a mineral such as quartz by using the following equation:

$$(^{18}O/^{16}O_{unknown})[(^{18}O/^{16}O_{ave\ std})/(^{18}O/^{16}O_{meas.\ std})] \quad (5)$$

where $^{18}O/^{16}O_{unknown}$ is the ratio measured on any mineral in a particular session, $^{18}O/^{16}O_{meas.\ std}$ is the ratio measured on quartz during the same session, and $^{18}O/^{16}O_{ave\ std}$ is a fixed ratio chosen for the quartz standard (the average of $^{18}O/^{16}O$ ratios measured on quartz over multiple sessions).

By using this approach, mass bias for a variety of minerals is usually reproducible at a level similar to analytical uncertainty (Fig. 8, Table 7). These results indicate that a single standard can be used for daily mass bias calibration once the general mass bias-matrix relationship is known, and allows mass bias-matrix effects between various minerals measured in different analytical sessions to be compared.

4.2.2. Oxygen mass bias in silicates

A number of general observations can be made on the relations between $\delta^{18}O_{bias}$, chemical composition, implanted Cs, and ion yields in silicate minerals:

(1) As has been previously noted [13,15], there is a relatively good correlation between mass bias and average atomic weight (Fig. 9).

(2) Within different mineral groups, there are systematic relationships between chemical composition and mass bias. Fe- (and Mn-) rich compositions are the least fractionated, Mg-rich compositions the most fractionated, and Ca compositions are intermediate. As the mass bias of Mn and Fe compositions are similar, and Mn is typically a minor component, it can be considered equivalent to Fe in most minerals ($X_{Mn/(Fe+Mn)}$ <10‰). In garnet (and the orthosilicates olivine and monticellite) the change in mass bias as a function of atomic weight is much less between Mg and Ca compositions when compared to compo-

Table 7
Oxygen isotopes measured on silicate, some carbonate, and oxide phases [$^{18}O/^{16}O_{meas}$: Average raw ratio measured on each mineral, δ_{bias}: Instrumental mass bias calculated on the average raw ratio in per mil (see text). error: Reproducibility of δ_{inst} based on the standard deviation of n measurements. δ_{norm}: Instrumental mass bias normalized to a value of −73.8‰ for quartz (SiO_2) to allow intersession comparisons (see text)]

Date	Sample	n	$^{18}O/^{16}O_{meas}$	δ_{bias} (‰)	Error (‰)	δ_{norm} (‰)
4-20-94	Bz Qtz	3	1.8947	−75.4	0.7	
4-20-94	SP Fsp	8	1.8796	−71.9	1.4	−70.4
5-2-94	Bz Qtz	6	1.9021	−71.7	1.1	
5-2-94	UT Cc	6	1.8829	−68.0	1.0	−66.0
5-3-94	Bz Qtz	7	1.9190	−63.5	1.5	
5-3-94	UT Cc	6	1.9093	−55.1	1.4	−65.4
5-4-94	Bz Qtz	4	1.8959	−74.8	1.3	
5-4-94	437 Px	3	1.8693	−72.7	1.2	−71.7
5-5-94	Bz Qtz	5	1.9008	−72.4	1.1	
5-5-94	GM Gnt	4	1.8965	−60.0	1.6	−61.5
5-5-94	183 Px	4	1.8797	−68.4	0.9	−69.8
5-6-94	Bz Qtz	6	1.9020	−71.8	1.0	
5-6-94	SP Fsp	4	1.8825	−70.5	0.6	−72.5
5-6-94	183 Px	6	1.8800	−68.2	0.9	−70.2
8-12-94	Bz Qtz	7	1.8950	−75.2	0.7	
8-12-94	UT Cc	6	1.8869	−66.1	0.4	−64.7
8-12-94	SP Fsp	5	1.8816	−70.9	0.7	−69.5
8-12-94	PyQ Gnt	6	1.8725	−71.3	0.6	−69.9
8-12-94	Gspd Gnt	5	1.8857	−66.6	0.5	−65.2
8-12-94	Brk Gnt	6	1.9194	−49.2	0.9	−47.7
8-12-94	Am Fsp	6	1.8797	−72.4	0.6	−71.0
8-16-94	Bz Qtz	8	1.8974	−74.0	0.7	
8-16-94	UT Cc	6	1.8871	−66.0	0.4	−65.8
8-16-94	SP Fsp	6	1.8841	−69.7	0.7	−69.5
8-16-94	Carr Qtz	4	1.9145	−74.2	0.9	−74.0
8-17-94	Bz Qtz	6	1.9039	−70.9	0.6	
8-17-94	SP Fsp	6	1.8856	−69.0	0.8	−71.9
8-31-94	Bz Qtz	8	1.8916	−76.9	1.1	
8-31-94	N-28 Qtz	3	1.8682	−77.2	0.9	−74.1
8-31-94	Carr Qtz	4	1.9085	−77.1	0.5	−74.0
8-9-94	Bz Qtz	8	1.9072	−69.3	0.8	
8-9-94	183 Px	6	1.8762	−70.1	0.9	−74.6
9-27-94	Bz Qtz	5	1.8891	−78.1	0.5	
9-27-94	UT Cc	5	1.8666	−70.6	0.8	−66.3
9-27-94	SP Fsp	3	1.8752	−74.1	0.7	−69.8
9-27-94	SC Oliv	3	1.8730	−71.0	0.2	−66.7
9-27-94	PyQ Gnt	4	1.8648	−75.1	1.2	−70.8
9-27-94	Ont Fsp	3	1.8815	−71.3	1.1	−66.9
9-27-94	ND Cc	3	1.8694	−77.3	0.3	−73.0
9-27-94	Mont	4	1.9077	−69.0	1.1	−64.7
9-27-94	Kyan	3	1.8641	−77.7	0.5	−73.5
9-27-94	Gspd Gnt	3	1.8809	−69.0	0.7	−64.6
9-27-94	FeD Cc	3	1.8910	−58.9	0.2	−54.5
9-27-94	DM Cc	3	1.8436	−79.3	0.5	−75.1
9-27-94	183 Px	4	1.8700	−73.2	0.8	−68.9
9-27-94	Casc Px	3	1.8977	−73.0	0.7	−68.7
9-27-94	Brk Gnt	3	1.9107	−53.5	0.4	−49.1
9-27-94	Am Fsp	3	1.8720	−76.2	0.6	−71.9
9-27-94	438 Gnt	3	1.8778	−66.3	0.5	−62.0

continued

Table 7
(continued)

Date	Sample	*n*	$^{18}O/^{16}O_{meas}$	δ_{bias} (‰)	Error (‰)	δ_{norm} (‰)
9-28-94	Bz Qtz	8	1.8872	−79.0	0.5	
9-28-94	SHR4 Rt	4	1.9367	−36.9	0.9	−31.4
9-28-94	LP204 Mt	3	1.9348	−43.6	0.9	−38.2
9-28-94	MAn Fsp	3	1.8672	−77.7	0.8	−72.5
9-28-94	GM Gnt	3	1.8827	−66.9	1.0	−61.6
9-28-94	Brk Gnt	3	1.9086	−54.5	1.0	−49.2
9-28-94	437 Gnt	3	1.8731	−70.5	0.1	−65.3
11-1-94	Bz Qtz	4	1.9056	−70.0	1.0	
11-1-94	BOG Qtz	3	1.8853	−71.2	0.1	−73.8
11-1-94	Sps Gnt	4	1.9172	−49.0	0.9	−51.7
11-1-94	PyQ Gnt	3	1.8728	−71.1	0.7	−73.7
11-1-94	Mex Gnt	4	1.8977	−61.9	0.9	−64.5
11-1-94	J546 Gnt	3	1.8879	−61.1	0.9	−63.7
11-1-94	JL1 Gnt	3	1.8875	−63.8	0.3	−66.4
11-1-94	Gspd Gnt	4	1.8908	−64.1	0.8	−66.7
11-1-94	GM Gnt	3	1.8956	−60.5	0.1	−63.1
11-1-94	CrA Px	4	1.8805	−66.8	0.8	−69.4
11-1-94	Brk Gnt	3	1.9247	−46.5	1.0	−49.2
11-1-94	GrA Gnt	3	1.8786	−66.4	1.4	−69.0
11-1-94	AZ Gnt	3	1.8871	−62.8	1.3	−65.4
11-1-94	438 Gnt	3	1.8903	−60.1	1.5	−62.7
11-3-94	BOG Qtz	5	1.8890	−69.4	0.5	
11-3-94	J147 Gnt	3	1.8899	−62.5	0.4	−66.9
11-3-94	1147 Gnt	3	1.8872	−62.0	0.1	−66.5
11-3-94	JH1 Gnt	3	1.8890	−63.0	1.2	−67.4
11-3-94	JE3 Gnt	4	1.8988	−59.6	0.4	−64.1
11-3-94	G143 Gnt	3	1.8994	−59.6	0.3	−64.1
11-3-94	GM Gnt	3	1.8975	−59.5	1.3	−64.0
11-3-94	CrA Px	2	1.8872	−63.4	0.6	−67.9
11-3-94	Brk Gnt	3	1.9281	−44.8	1.4	−49.4
12-13-94	BOG Qtz	1	1.8950	−66.4	0.8	
12-13-94	Mex Gnt	2	1.9037	−60.6	0.9	−68.0
12-13-94	And Gnt	9	1.9000	−49.0	0.8	−56.5
12-15-94	BOG Qtz	2	1.8788	−74.4	0.1	
12-15-94	SL18 Oliv	1	1.8720	−71.6	1.0	−71.0
12-15-94	Mont	2	1.9165	−64.7	0.0	−64.1
12-15-94	ESt Oliv	2	1.8779	−60.8	1.4	−60.1
12-15-94	CM Oliv	3	1.8701	−74.6	1.2	−74.0
12-15-94	CrA Px	2	1.8803	−66.8	1.6	−66.2
12-19-94	BOG Qtz	8	1.8732	−77.2	0.6	
12-19-94	SP Fsp	4	1.8723	−75.2	0.4	−71.9
12-19-94	Shrp Fsp	5	1.8669	−76.7	1.1	−73.3
12-19-94	SHR6 Fsp	4	1.8762	−73.6	0.6	−70.3
12-19-94	OLa Fsp	4	1.8637	−75.2	0.7	−71.8
12-19-94	MBy Fsp	4	1.8679	−73.9	0.9	−70.5
12-19-94	MAn Fsp	4	1.8688	−76.9	0.9	−73.5
12-19-94	JAn Fsp	4	1.8670	−74.1	0.6	−70.7
12-19-94	CrA Px	4	1.8663	−73.8	0.8	−70.4
12-19-94	Am Fsp	4	1.8742	−75.1	1.0	−71.7
2-21-95	BOG Qtz	7	1.8512	−88.0	0.9	
2-21-95	Spw Oliv	3	1.8573	−76.4	1.0	−62.0

continued

Table 7
(continued)

Date	Sample	*n*	$^{18}O/^{16}O_{meas}$	δ_{bias} (‰)	Error (‰)	δ_{norm} (‰)
2-21-95	SL18 Oliv	3	1.8528	−80.8	1.3	−66.5
2-21-95	SC Oliv	4	1.8564	−79.3	0.8	−64.9
2-21-95	Mont	4	1.8834	−80.9	1.0	−66.5
2-21-95	J147 Oliv	5	1.8493	−82.5	0.8	−68.2
2-21-95	ESt Oliv	4	1.8493	−75.1	0.7	−60.6
2-21-95	CM Oliv	4	1.8462	−86.4	0.3	−72.2
2-21-95	CrA Px	4	1.8547	−79.5	0.3	−65.2
2-21-95	1888 Oliv	4	1.8574	−78.4	0.5	−64.0
2-21-95	Ami Oliv	4	1.8641	−81.7	1.2	−67.3
2-21-95	All Oliv	5	1.8455	−86.2	1.2	−72.0
4-11-95	BOG Qtz	6	1.8772	−75.2	0.5	
4-11-95	And Gnt	4	1.8845	−56.8	0.8	−55.4
4-11-95	Brk Gnt	4	1.9185	−49.6	0.4	−48.2
4-11-95	438 Gnt	4	1.8863	−62.1	0.9	−60.7
4-11-95	PyQ Gnt	4	1.8689	−73.1	1.1	−71.7
4-11-95	Gspd Gnt	4	1.8861	−66.4	0.5	−65.0
4-11-95	GrA Gnt	4	1.8717	−69.8	0.6	−68.4
4-11-95	Mex Gnt	4	1.8892	−67.7	0.4	−66.3
4-19-95	BOG Qtz	12	1.8850	−71.4	1.0	
4-19-95	Sps Gnt	4	1.9229	−46.2	0.3	−48.7
4-19-95	PyQ Gnt	4	1.8789	−68.1	0.2	−70.6
4-19-95	Mex Gnt	4	1.9000	−62.4	0.6	−64.9
4-19-95	J147 Gnt	4	1.8899	−62.5	0.5	−64.9
4-19-95	1146 Gnt	4	1.8850	−63.1	0.6	−65.6
4-19-95	J546 Gnt	4	1.8847	−62.7	0.3	−65.2
4-19-95	JL1 Gnt	4	1.8884	−63.3	0.3	−65.8
4-19-95	JH1 Gnt	4	1.8884	−63.3	1.0	−65.8
4-19-95	JE3 Gnt	4	1.8987	−59.7	0.4	−62.2
4-19-95	Gspd Gnt	4	1.8976	−60.7	0.5	−63.2
4-19-95	G143 Gnt	4	1.9020	−58.3	1.0	−60.8
4-19-95	GM Gnt	4	1.9039	−56.4	1.0	−58.8
4-19-95	Brk Gnt	4	1.9290	−44.4	0.5	−46.9
4-19-95	GrA Gnt	4	1.8844	−63.5	0.8	−66.0
4-19-95	AZ Gnt	4	1.8937	−59.6	1.0	−62.0
4-19-95	And Gnt	4	1.8912	−53.4	1.1	−55.9
4-19-95	438 Gnt	4	1.8948	−57.9	0.8	−60.4
4-19-95	Mel Gnt	4	1.9149	−52.9	0.8	−55.4
4-19-95	Mal Gnt	4	1.9076	−57.4	1.7	−59.9
4-19-95	May Gnt	4	1.9136	−57.6	1.2	−60.0

sitions varying between Fe (+Mn) and Ca end members (Table 7). Similar relationships are observed in carbonate minerals.

(3) Within mineral groups dominated by Mg–Ca–Fe (+Mn) compositional variations, there is good correlation between the atomic proportion of Fe (+Mn) and mass bias, provided the proportion of Mn remains small (Fig. 10).

(4) There is a relatively good correlation between decreasing mass bias and an increase in the secondary ion intensity of $^{133}Cs^-$ relative to the $^{16}O^-$ secondary ion intensity, normalized to the total amount of oxygen present in the sample ($^{133}Cs^-/^{16}O^-$) (Fig. 11).

(5) There is a strong correlation between atomic Fe+Mn (relative to Fe–Mg–Ca–Mn) and $^{133}Cs^-/^{16}O^-$ in garnets and olivines (Fig. 12). There is also a good correlation between $^{133}Cs^-/^{16}O^-$ and percentage of atomic Na in feldspars along the Na–Ca

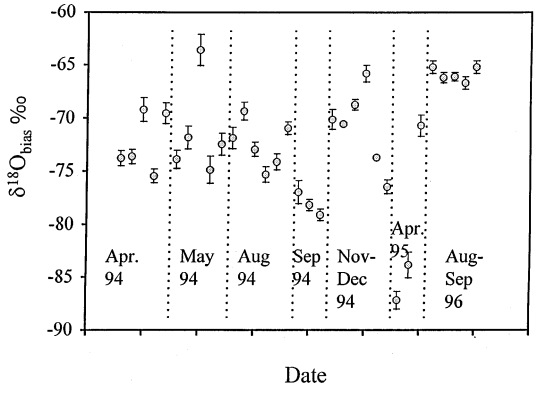

Fig. 7. Average $\delta^{18}O_{bias}$ values for quartz (SiO_2) measured over a three-year period.

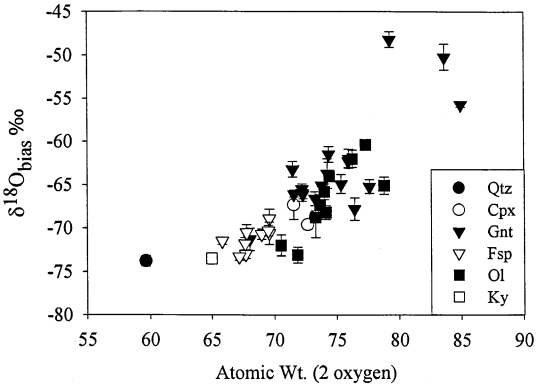

Fig. 9. $\delta^{18}O_{bias}$ as a function of the normalized atomic weight of different silicate minerals (modified from [13]). Abbreviations are: Qtz—quartz; Cpx—clinopyroxene; Gnt—garnet; Fsp—feldspar; Ol—olivine; Ky—kyanite (see Table 3 for compositions). Error bars represent 1σ reproducibility.

compositional join; K feldspars are offset from the main trend (Fig. 13).

(6) There is no apparent correlation between oxygen ion yield (counts $^{16}O^-$ per s per nA of primary current) and either mass bias (Fig. 14) or mineral chemistry, even within individual mineral groups.

4.2.3. Oxygen and carbon mass bias in carbonates

Analysis of carbonate minerals allows study of both carbon and oxygen mass bias behavior in the same matrix. As a wide variety of cations can substitute into the carbonate structure, there are a number of carbonate end-member minerals. We have noted both similarities and differences between oxygen isotope mass bias behavior in silicates and that observed for oxygen (and carbon) isotopes in carbonates:

(1) Oxygen and carbon mass bias in different matrices is relatively well correlated, although there is some scatter, particularly for Zn carbonate (Fig. 15).

(2) There is a general correlation between decreasing oxygen mass bias and increasing atomic weight, although there are significant variations from the general trend, particularly for carbonates with large concentrations of Pb and Ba (Fig. 16). Similar trends

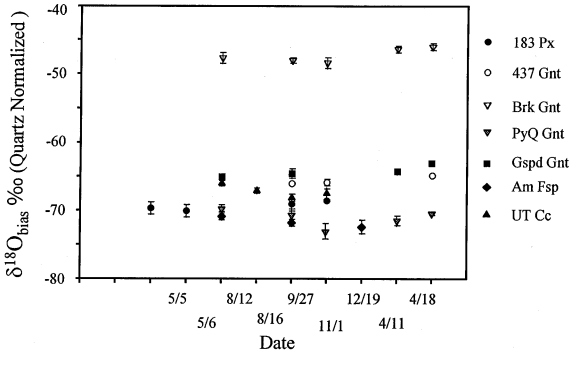

Fig. 8. $\delta^{18}O_{bias}$ values for different minerals measured in different analytical sessions over approximately one year (Table 7). Data normalized to the mass bias measured on quartz (SiO_2). Error bars represent 1σ reproducibility.

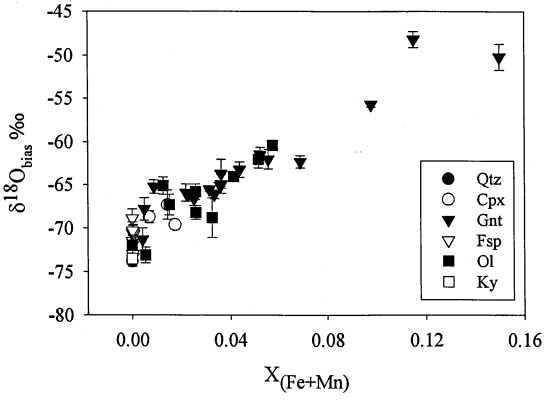

Fig. 10. $\delta^{18}O_{bias}$ as a function of the atomic proportion of Fe+Mn in silicate minerals. Abbreviations after Fig. 9. Error bars represent 1σ reproducibility.

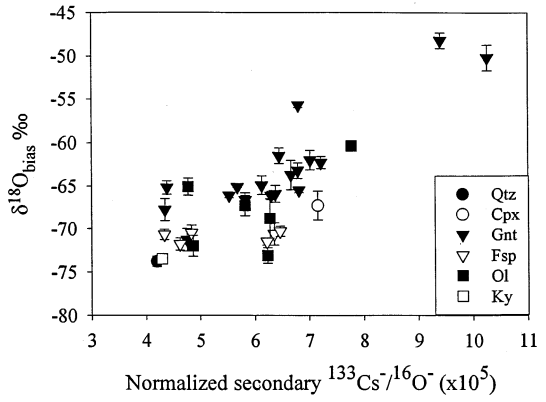

Fig. 11. $\delta^{18}O_{bias}$ as a function of the secondary $^{133}Cs^-/^{16}O^-$ count ratio (normalized to proportion of atomic oxygen) in silicate minerals. Abbreviations after Fig. 9. Error bars represent 1σ reproducibility.

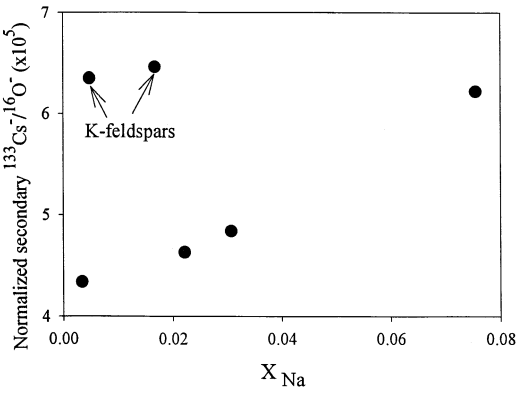

Fig. 13. Secondary ion $^{133}Cs^-/^{16}O^-$ ratio (normalized to proportion of atomic oxygen) as a function of atomic Na in feldspars.

are observed for $\delta^{13}C_{bias}$, although there is more scatter.

(3) Relative mass bias relations among Mg, Ca, Fe, and Mn compositions are similar to those observed in silicates: Mg compositions are the most fractionated, Fe (+Mn) the least fractionated, and Ca compositions have intermediate fractionations closer to those of Mg compositions.

(4) Within minerals dominated by substitutions involving Mg, Ca, Fe, and Mn, there is a reasonable correlation between X_{Fe+Mn} and oxygen mass bias, as is observed in silicates (Fig. 17). However, the relationship is not linear, and utilizing X_{Fe} to estimate mass bias [e.g., 30] could lead to significant errors in accuracy, particularly for Mg-rich compositions.

(5) In contrast to silicates, mass bias in carbonates is not well correlated with the ratio of the secondary ion intensities of $^{133}Cs^-$ and $^{16}O^-$ (Fig. 18). There is also little correlation between mass bias and the $^{133}Cs^-/^{12}C^-$ ratio.

(6) There is a good correlation between oxygen ion yield and $\delta^{18}O_{bias}$ (Fig. 19). The correlation between oxygen ion yield and $\delta^{13}C_{bias}$ is similar but more scattered.

(7) For carbonates in the Mg–Ca–Pb–Ba–Sr sys-

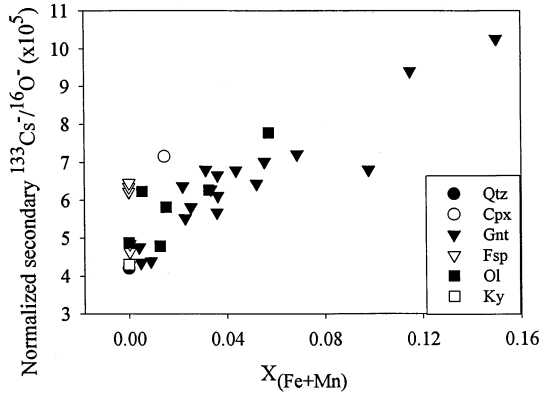

Fig. 12. Secondary ion $^{133}Cs^-/^{16}O^-$ ratio (normalized to proportion of atomic oxygen) as a function of atomic Fe+Mn in silicate minerals. Abbreviations after Fig. 9.

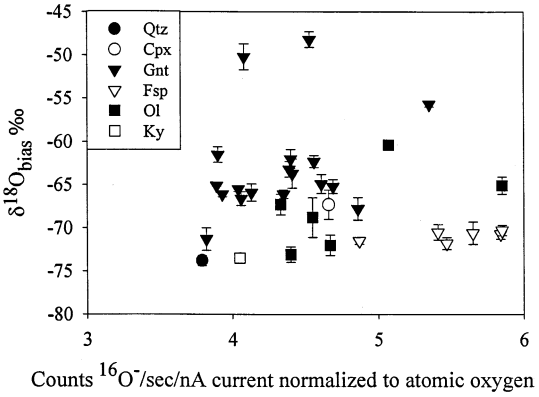

Fig. 14. $\delta^{18}O_{bias}$ in silicates as a function of $^{16}O^-$ ion yield. Error bars represent 1σ reproducibility.

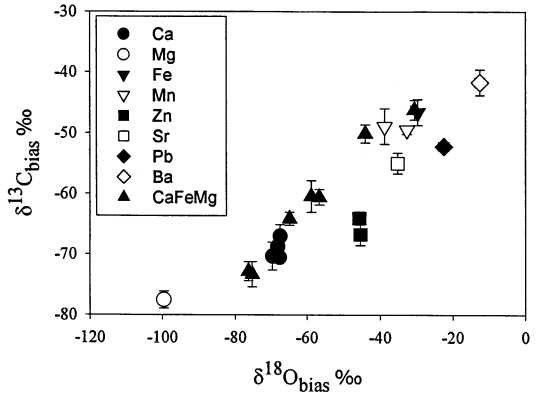

Fig. 15. Correlation between $\delta^{18}O_{bias}$ and $\delta^{13}C_{bias}$ values for carbonates. CaFeMg indicates solid solutions among Ca–Mg–Fe–Mn components. Other minerals have >85‰ cation proportion of the indicated end-member component. Error bars represent 1σ reproducibility.

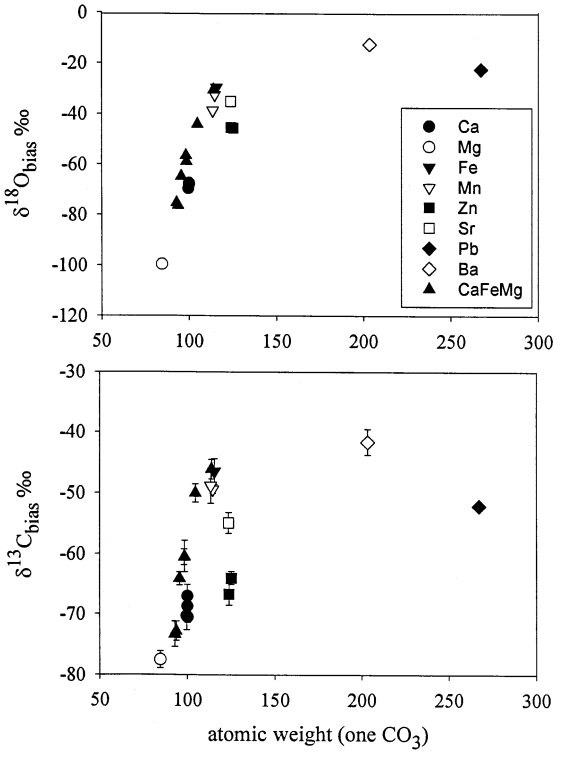

Fig. 16. Carbonate $\delta^{18}O_{bias}$ and $\delta^{13}C_{bias}$ values as a function of atomic weight normalized to one CO_3. Abbreviations after Fig. 15. Error bars represent 1σ reproducibility.

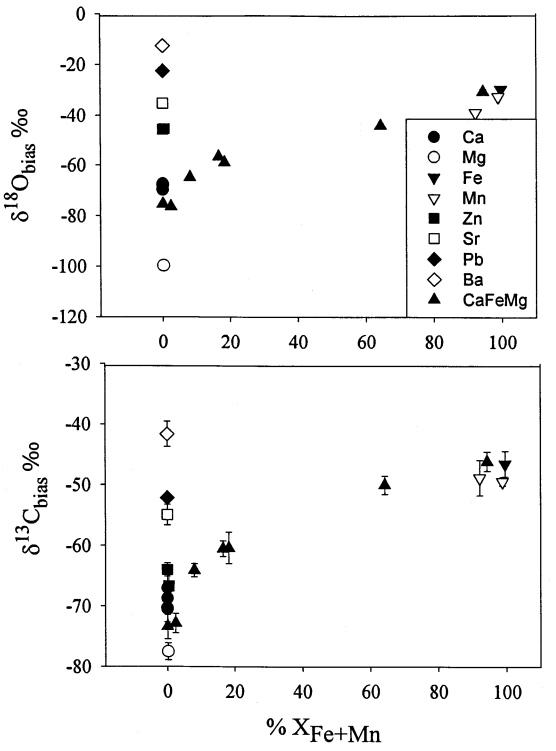

Fig. 17. Carbonate $\delta^{18}O_{bias}$ and $\delta^{13}C_{bias}$ values as a function of atomic proportion of Fe+Mn. Abbreviations after Fig. 15. Error bars represent 1σ reproducibility.

tem, and for Ca–Mg carbonates with moderate substitution of Mn and Fe (Fig. 20), there is a good correlation between $\delta^{18}O_{bias}$ and carbon ion yield. However, near end-member Mn and Fe carbonates fall significantly off this trend, as do Zn carbonates. Again with the exception of Zn carbonate, similar relations are observed between $\delta^{13}C_{bias}$ and carbon ion yields. The mass bias behavior of Zn carbonate appears to be strongly element dependent; $\delta^{18}O_{bias}$ values are similar to Fe and Mn end-member carbonates, but $\delta^{13}C_{bias}$ values are more similar to Ca–Mg carbonates (Fig. 20).

(8) As indicated by comparison of Figs. 16 and 19, there is a general trend between increasing oxygen ion yield and increasing average atomic weight.

(9) The $\delta^{13}C_{bias}$ value of a pure carbon target (graphite, −46.5‰) is intermediate in the range observed for carbonates.

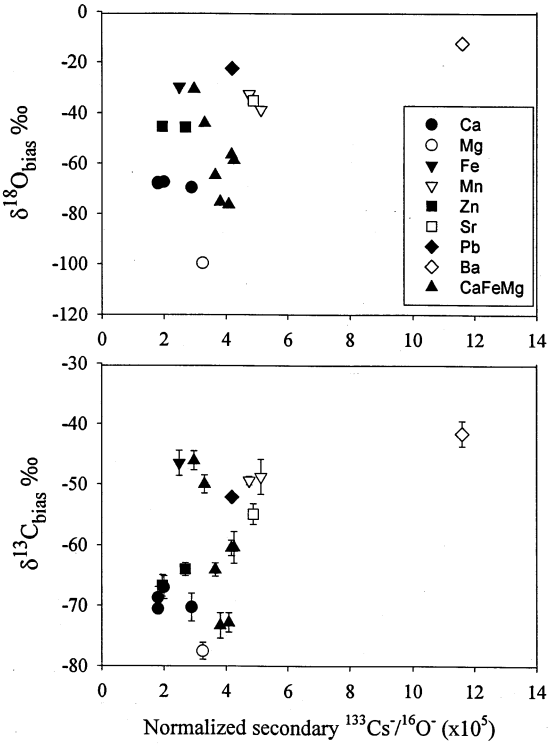

Fig. 18. Carbonate $\delta^{18}O_{bias}$ and $\delta^{13}C_{bias}$ values as a function of $^{133}Cs^{-}/^{16}O^{-}$ ion yield. Abbreviations after Fig. 15. Error bars represent 1σ reproducibility.

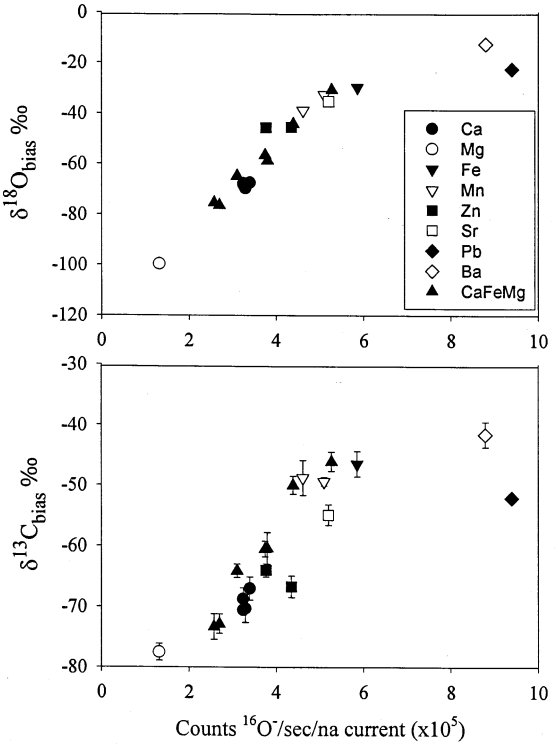

Fig. 19. Carbonate $\delta^{18}O_{bias}$ and $\delta^{13}C_{bias}$ values as a function of oxygen ion yield. Abbreviations after Fig. 15. Error bars represent 1σ reproducibility.

5. Discussion

5.1. Mass bias models

The instrumental contribution to mass bias can be controlled by the operator, making corrections relatively simple. However, isotopic fractionation occurring during sputtering/ionization also depends upon the target material, and correcting for these matrix dependent effects is more problematic. Sputtering theory suggests that a number of target-dependent factors will determine mass fractionation, including binding energy of the surface atoms (bond strength), the mass ratio of the isotopes, the work function of the surface, emission angle, ionization potential, and kinetic energy of both the sputtering and sputtered ions [e.g., 27,31–35]. A variety of sputtering/ionization mechanisms have been proposed [e.g., 35–44]. Mass fractionation behavior in ionic solids is predicted fairly well by a bond-breaking model [e.g. 36], and that of metals and semiconductors by an electron tunneling model [e.g. 35]. However, none of these models predicts the general observation that light isotope enrichment increases with secondary ion energy $>$30–50 eV. Several workers have suggested that there are competing mechanisms of ion production [e.g. 10,42,44], with bond-breaking or electron tunneling mechanisms dominant for low-energy secondary ions and higher energy ion formation dominated by a collisional mechanism.

The development of general sputtering/ionization models have typically been limited to simple chemical matrices and application of these models to geological materials has been hampered by the chemical complexity of minerals and glasses. However, empirical calibrations and predictive modeling of isotopic frac-

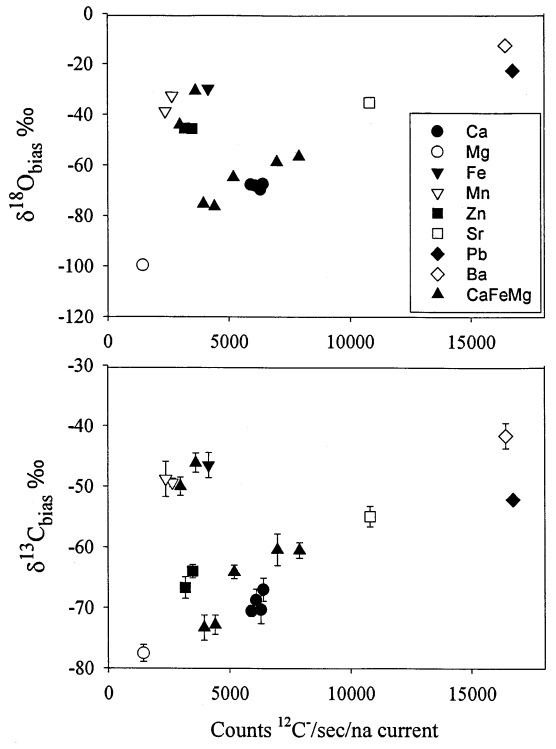

Fig. 20. Carbonate $\delta^{18}O_{bias}$ and $\delta^{13}C_{bias}$ values as a function of carbon ion yield. Abbreviations after Fig. 15. Error bars represent 1σ reproducibility.

tionations arising from matrix effects have been undertaken for a number of light stable isotopes including hydrogen [10,11], oxygen [13,15,29,45–49], and boron [9]. In the following discussion, the application of these empirical models will be tested by using the data presented here. Most silicate and carbonate minerals are complex solid solutions and considerable effort has focused on the development of oxygen isotope mass bias models for these phases. As matrix effects are thought to be simpler for high-energy secondary ions [e.g. 16,29] results obtained for oxygen isotopes in silicates, and oxygen and carbon isotopes in carbonates by using extreme energy filtering, will be discussed first. These results will be compared to the limited amount of data available from other laboratories for oxygen isotope ratios measured on silicates and carbonates by using low-energy secondary ions.

5.2. Isotopic mass bias of oxygen in silicates using high-energy secondary ions

Variations in mass bias as a function of matrix composition are large when using extreme energy filtering, even within single mineral groups; for example, values of $\delta^{18}O_{bias}$ vary 20 to 80‰ between Fe and Mg end-member compositions, depending on the mineral group. This range is far larger than the natural variations of $\delta^{18}O$ values in most geologic systems. Therefore, an accurate method of correcting measured isotope ratios for matrix effects is critical for the application of SIMS methods.

In their paper demonstrating the extreme energy filtering method for the analysis of oxygen isotopes, Hervig et al. [13] suggested that mass bias was strongly correlated with the oxygen-normalized formula weight of a wide variety of minerals. This observation was based on the analysis of a limited number of mineral phases with restricted chemical compositions. Further work on minerals with a wider range of chemical composition has demonstrated that, although the general correlation of decreasing instrumental fractionation associated with increasing formula weight is relatively strong, this approach can result in accuracy errors greater than 10‰ for some minerals [15; Fig. 9]. Despite differences in the magnitude by which $\delta^{18}O_{bias}$ varies, there are systematic correlations between mass bias and chemical composition for a variety of silicate (garnet, olivine, pyroxene) and carbonate mineral groups. Mg-rich compositions give consistently higher mass biases; Fe- and Mn-rich compositions consistently lower. Ca-rich compositions are similar to, but less fractionated than, Mg-rich compositions [45]. These observations suggest that mass bias measured by using high kinetic energy secondary ions might be a relatively simple function of chemical composition.

For the mineral olivine [a compositionally simple $(Fe,Mg)_2SiO_4$ solid-solution mineral] $\delta^{18}O_{bias}$ varies as a linear function of chemical composition (within analytical uncertainty) along significant portions of the Fe–Mg binary join (Fig. 21), although this relation apparently becomes nonlinear at Fe-rich compositions [29]. Similar linear behavior is also observed along

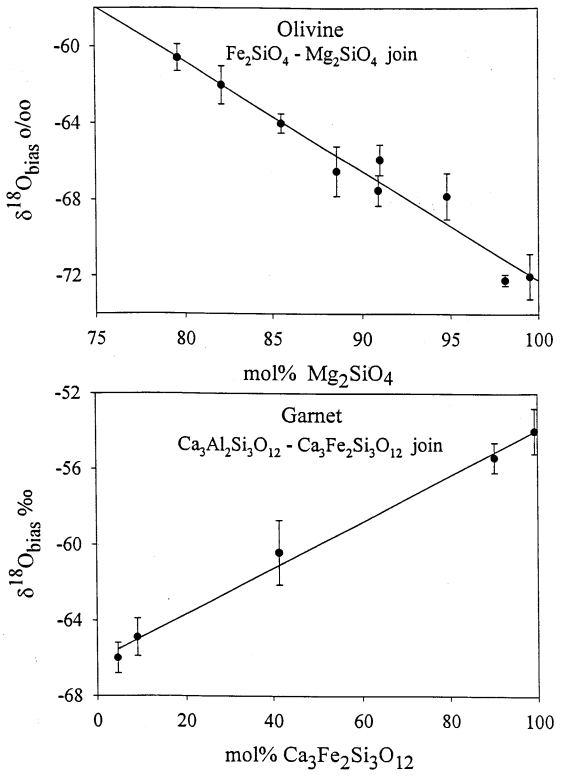

Fig. 21. Olivine $\delta^{18}O_{bias}$ values as a function of atomic proportion of Mg normalized to Fe–Mg along the compositional binary. Garnet $\delta^{18}O_{bias}$ values as a function of atomic proportion of the Fe component normalized to Fe–Al along the andradite-grossular compositional binary. Error bars represent 1‰ reproducibility of repeated (3–5) measurements on each standard.

the Fe–Al binary join between andradite ($Ca_3Fe_2Si_3O_{12}$) and grossular ($Ca_3Al_2Si_3O_{12}$) garnets (Fig. 21). This suggests that $\delta^{18}O_{bias}$ can be calibrated by linear interpolation along significant portions of the binary chemical join. For many minerals, this may be the simplest approach to calibration, mainly requiring enough standards to test the assumption of linear behavior.

This approach can be extended to mineral systems with more complex solid solutions if mass bias is assumed to vary linearly along all binary chemical joins. By using this approach, the percentage of each end-member component in an "unknown" sample is calculated based on the major element analysis (typically determined by electron microprobe). The mass bias for each end-member composition is determined by analyzing standards with near end-member compositions. The mass bias of the unknown is then determined by multiplying the mass bias for each end-member composition by the atom percentage of that composition in the unknown, and summing the results for each end-member [46] by using the equation

$$\beta_{inst} = \Sigma(n_x\beta_x) \quad (6)$$

where n is the atomic fraction of a chemical end-member x and β_x is the appropriate mass bias for that end-member composition.

This empirical model can be tested by using garnet, a complex solid-solution silicate for which we have analyzed a variety of compositions. A wide range of potential garnet compositions exists, with principal substitution occurring in the eightfold and sixfold coordination sites $(Fe,Mg,Ca,Mn)_3(Fe,Cr,Al)_2Si_3O_{12}$. There are six major end-member compositions: almandine ($Fe_3Al_2Si_3O_{12}$), pyrope ($Mg_3Al_2Si_3O_{12}$), grossular ($Ca_3Al_2Si_3O_{12}$), spessartine ($Mn_3Al_2Si_3O_{12}$), andradite ($Ca_3Fe_2Si_3O_{12}$), and uvarovite ($Ca_3Cr_2Si_3O_{12}$). Most natural garnets, and most of the garnets we analyzed, have compositions that are >90‰ in the $(Fe,Ca,Mg)_3Al_2Si_3O_{12}$ ternary, allowing much of the chemical variability to be accounted for by using only these three end-member compositions. For the purposes of these calculations, we have used Brk, PyQ, and GrA (Table 3) to calculate the Fe-, Mg-, and Ca-end-member mass biases. The results for these calculations are summarized in Table 8. For samples with minimal (<15‰) spessartine, andradite, and uvarovite components, the agreement between the predicted and measured mass biases is typically within 1.5‰, similar to analytical uncertainty. Addition of other chemical end members spessartine (Sp) and andradite (An) to the calculation improves the fit between predicted and measured end-member biases (Table 8). The fit can also be slightly improved by using analyses collected during a single analytical session, rather than by using the average values obtained over the entire year-long analytical period. Similar fits are obtained if all the minerals are used to

Table 8
$\delta^{18}O_{bias}$ calculated for garnets assuming linear mass bias behavior between end members [Mass bias calculated by multiplying the atom percentage of each chemical end member in each garnet by the appropriate end-member mass bias determined by measuring a near end-member composition garnet. Al—Almandine (Brk Std), Gr—Grossular (GrA Std), Py—Pyrope (PyQ Std), An—Andradite (And Std), Sp—Spessartine (Sps Std). Both the calculated and measured mass biases use the average value for each mineral obtained over the ~1 year analytical period. The end-member $\delta^{18}O_{bias}$ were: Py = −72.5‰, Al = −42.0‰, Gr = −68.7‰, Sp = −50.7‰, An = −55.5‰]

	Gr, Py, Al $\delta^{18}O_{bias}$‰	Gr, Py, Al, An $\delta^{18}O_{bias}$‰	Gr, Py, Al, Sp $\delta^{18}O_{bias}$‰	Gr, Py, Al, Sp, An $\delta^{18}O_{bias}$‰	Measured $\delta^{18}O_{bias}$‰
437	−65.8	−65.8	−65.7	−65.7	−65.5
Gspd	−63.4	−63.4	−63.3	−63.3	−64.9
PyQ	−71.7	−71.7	−71.7	−71.7	−71.7
438	−61.2	−61.2	−61.1	−61.1	−61.5
Brk	−48.4	−48.4	−48.4	−48.4	−48.4
GM	−58.1	−58.1	−58.0	−58.0	−60.5
JE3	−63.4	−63.4	−63.3	−63.3	−63.2
J546	−64.2	−64.2	−64.1	−64.1	−65.1
J147	−67.6	−67.7	−67.5	−67.6	−65.9
JH1	−67.0	−67.0	−66.9	−66.9	−66.6
AZ	−64.8	−64.9	−64.7	−64.7	−63.7
Mex	−67.3	−67.6	−67.3	−67.6	−66.2
JL1	−67.6	−67.7	−67.5	−67.6	−66.1
G143	−60.8	−60.8	−60.7	−60.7	−62.0
1146	−65.1	−65.2	−65.0	−65.1	−66.1
GrA	−67.8	−67.8	−67.8	−67.8	−67.8
Sps	−43.3	−43.3	−50.2	−50.2	−50.2
And	−58.3	−55.7	−58.3	−55.6	−55.7
Mel	−58.3	−56.8	−58.3	−56.8	−55.4
Mal	−48.3	−61.2	−48.0	−61.2	−60.9
May	−56.8	−56.8	−59.8	−59.8	−60.0

determine end-member mass biases by multiple regression. These results indicate that, in at least some mineral systems, if standards bracketing the chemical compositions are available, matrix effects can be linearly interpolated with accuracies similar to the precision of individual measurements. This approach is limited by the fact that mass bias is not a linear function of chemical composition in all mineral systems and by the availability of standards.

A number of workers have suggested that the shapes of high-energy secondary ion yield curves are nearly exponential and are consistent with distributions expected by energy transfer in the collision cascade (e.g. [10,28,31,42,50]). This has led to the development of a predictive mass bias model based on relative differences in the efficiency of energy transfer between light and heavy isotopes in the collision cascade [29]. Although multiple collisions are required to eject a secondary ion into the mass spectrometer, by using the assumption that the sputter/ionization process results solely from kinetic energy transfer, the isotope fractionation effect will result from the difference in ionization efficiency (γ) for the two isotopes in the final collision that ejects the ion of interest from the sample

$$\gamma^H/\gamma^L = \{(M_I M_H)/(M_I + M_H)^2\}/\{(M_I M_L)/(M_I + M_L)^2\} \quad (7)$$

where M is the mass of: L—the light isotope; H—the heavy isotope; and I—the colliding ion that ejects the ion of interest [29]. To account for the chemical variation in geological matrices, Eiler et al. [29] proposed that the mass bias efficiencies will sum linearly based on the atomic proportion of each element (as proposed for the end-member model

discussed earlier). In addition, they suggested that there will be an additional factor for each element arising from variable collision efficiency, and that this factor would scale as $1/r^2$ where r is the atomic radius of colliding ion. Therefore, the mass bias should be predicted by using the equation

$$\gamma^{H}/\gamma^{L} = \Sigma(n_I\gamma_H r_I^{-2})\Sigma(n_I\gamma_L r_I^{-2}) \quad (8)$$

where n is the atomic percentage of colliding atoms (I) per formula unit and r the radius of ion I.

In practice, application of this equation is somewhat arbitrary, because (1) atomic radii within mineral matrices are poorly constrained, such that use of covelant, ionic, and atomic radii lead to widely varying predictions; and (2) use of radius as a proxy for a collisional cross section is uncertain. The equation also assumes that the amount of implanted primary ion is essentially constant from one matrix to another and thus can be ignored. Empirical application with covalent radii produced a good correlation between predicted and measured mass bias among 17 silicate minerals [29]. Eiler et al. [29] also noted that projection of the relation between measured and predicted mass bias to the composition of a pure oxygen target gave a $\delta^{18}O_{bias}$ value very close to −111‰, which is the value predicted by using the $Mass_{light}/Mass_{heavy}$ relation [43] observed for pure metals. This observation was used to suggest that there are no significant additional source of mass bias for high energy ions beyond those incorporated into the energy transfer model and they suggested that the model might successfully be used for the isotopic analysis of other elements utilizing high kinetic energy secondary ions [29].

By using the same equations to model our data set of forty-four silicate mineral compositions, we observe a relatively good correlation between the predicted and measured mass bias (Fig. 22). However, there is significant scatter, particularly for minerals in which major element variations are not within the Fe–Ca–Mg compositional fields, and inaccuracies of up to 5‰ could result if a "best fit" equation were applied to our data (Table 9). The absolute range in magnitude of the predicted mass bias is a factor of ten

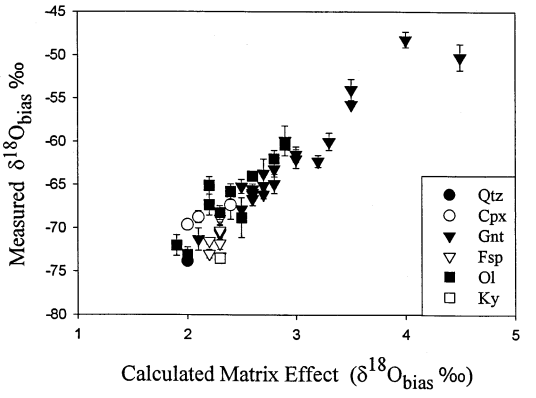

Fig. 22. Correlation between $\delta^{18}O_{bias}$ values measured on silicates and those predicted by using the kinetic energy sputtering model [29]. Abbreviations after Fig. 9. Error bars represent 1σ reproducibility.

smaller than the actual range of measured mass bias. In addition, this model predicts that mass bias values should be positive (heavy isotope enriched), whereas measured mass bias values are negative (light isotope enriched), indicating that formulation of the energy transfer model is incorrect. Application of this model to include carbonates, oxides, and a synthetic Ga–Ge–Gd (GGD) garnet results in very poor fits (Fig. 23), indicating that the model cannot be extended to nonsilicates.

The good correlation observed between the measured $^{133}Cs^-/^{16}O^-$ secondary ion ratio and $\delta^{18}O_{bias}$ in silicate minerals suggests a quantitative link between implanted Cs and mass bias (Fig. 11), and a direct relationship between higher average atomic weight and higher $^{133}Cs^-/^{16}O^-$ ratio. This could reflect that the average stopping distance for a Cs^+ primary ion is greater in a lighter matrix, so that, in a steady-state sputtering system, the relative amount of Cs in the near-surface will be lower. This could effect the mass bias in two ways. First, the heavier the colliding ion, the smaller the relative difference in energy transfer between two isotopes [e.g. Eq. (8)]. Therefore, increasing amounts of Cs in the near surface will decrease the degree of fractionation between the light and heavy isotope. Second, Cs implantation decreases the work function (and increases ion yield) for negative ions [e.g. 35]. Theoretical work [51,55] indicates

Table 9
Calculated $\delta^{18}O_{bias}$ for silicate minerals by using different models [Type—Mineral Group, Mont is monticellite, which is another orthosilicate similar to olivine. Std—See Table 3 for abbreviations: Meas. $\delta^{18}O_{bias}$ is the average measured $\delta^{18}O_{bias}$ (in ‰, Table 6). KE—Predicted $\delta^{18}O_{bias}$ by using results of the energy transfer model (see text). KE w/Cs—Predicted $\delta^{18}O_{bias}$ by using results of the energy transfer model incorporating Cs (see text). Chem—Predicted $\delta^{18}O_{bias}$ using atomic proportion of elements in each mineral (see text). Calc–Meas: The difference between the calculated and measured $\delta^{18}O_{bias}$]

Type	Std	Meas. $\delta^{18}O_{bias}$	KE $\delta^{18}O_{bias}$	Calc–Meas	KE w/Cs $\delta^{18}O_{bias}$	Calc–Meas	Chem $\delta^{18}O_{bias}$	Calc–Meas
Qtz	Qtz	−73.8	−72.2	−1.6	−71.9	−1.9	−74.4	0.6
Px	183	−69.6	−72.2	2.6			−66.8	−2.8
Px	Casc	−68.7	−71.1	2.4			−68.6	−0.1
Px	CrA	−67.3	−68.0	0.7	−67.6	0.3	−67.1	−0.2
Gnt	437	−65.5	−66.0	0.5	−63.8	−1.7	−66.0	0.5
Gnt	GM	−62.3	−59.8	−2.5	−61.1	−1.2	−59.1	−3.2
Gnt	Brk	−48.2	−51.5	3.3	−52.7	4.5	−49.9	1.7
Gnt	PyQ	−71.3	−71.1	−0.2	−71.9	0.6	−72.4	1.1
Gnt	Gspd	−64.9	−63.9	−1.0	−65.4	0.5	−63.8	−1.1
Gnt	438	−61.5	−61.8	0.3	−64.0	2.5	−61.9	0.4
Gnt	JE3	−63.2	−63.9	0.7	−63.5	0.3	−64.0	0.8
Gnt	J546	−65.1	−64.9	−0.2	−67.0	1.9	−64.8	−0.3
Gnt	J147	−65.9	−66.0	0.1	−65.1	−0.8	−65.7	−0.2
Gnt	JH1	−66.6	−66.0	−0.6	−67.0	0.4	−66.7	0.1
Gnt	AZ	−63.7	−64.9	1.2	−64.0	0.3	−64.7	1.0
Gnt	Mex	−65.2	−67.0	1.8			−66.6	1.4
Gnt	JL1	−66.1	−66.0	−0.1	−68.1	2.0	−66.2	0.1
Gnt	J143	−62.0	−61.8	−0.2	−62.1	0.1	−61.3	−0.7
Gnt	1146	−66.1	−64.9	−1.2	−65.4	−0.7	−65.7	−0.4
Gnt	GrA	−67.8	−67.0	−0.8	−71.9	4.1	−67.3	−0.5
Gnt	Sps	−50.2	−46.4	−3.8	−48.9	−1.3	−50.0	−0.2
Gnt	And	−55.7	−56.7	1.0	−62.7	7.0	−55.1	−0.6
Gnt	Mel	−55.4	−56.7	1.3			−55.5	0.1
Gnt	Mal	−59.9	−62.9	3.0			−61.1	1.2
Gnt	May	−60.0	−58.8	−1.2			−60.2	0.2
Fsp	Ont	−68.9	−69.1	0.2			−69.7	0.8
Fsp	Am	−71.5	−70.1	−1.4	−66.2	−5.3	−72.7	1.2
Fsp	MAn	−73.0	−70.1	−2.9			−72.0	−1.0
Fsp	SK	−70.6	−69.1	−1.5	−65.1	−5.5	−69.8	−0.8
Fsp	SP	−73.3	−69.1	−4.2			−71.8	−1.5
Fsp	JAn	−70.7	−69.1	−1.6	−72.2	1.5	−71.1	0.4
Fsp	OLa	−71.8	−69.1	−2.7	−71.3	−0.5	−71.6	−0.2
Fsp	MBy	−70.5	−69.1	−1.4	−70.5	0.0	−71.7	1.2
Fsp	SHR6	−70.3	−69.1	−1.2	−64.8	−5.5	−70.3	0.0
“Oliv”	Mont	−65.1	−70.1	5.0	−66.7	1.6	−65.9	0.8
Oliv	J147	−68.2	−69.1	0.9			−67.5	−0.7
Oliv	SC	−65.8	−68.0	2.2			−67.2	1.4
Oliv	SL18	−68.8	−67.0	−1.8	−67.0	−1.8	−66.2	−2.6
Oliv	All	−72.0	−73.2	1.2	−73.0	1.0	−72.3	0.3
Oliv	CM	−73.1	−72.2	−0.9	−73.5	0.4	−71.3	−1.8
Oliv	Ami	−67.3	−70.1	2.8	−69.2	1.9	−69.3	2.0
Oliv	1888	−64.0	−66.0	2.0			−64.5	0.5
Oliv	Spw	−62.0	−63.9	1.9			−62.3	0.3
Oliv	ESt	−60.4	−62.9	2.5	−61.3	0.9	−61.2	0.8
Kyan	Ky	−73.5	−69.1	−4.4	−72.4	−1.1	−73.4	−0.1

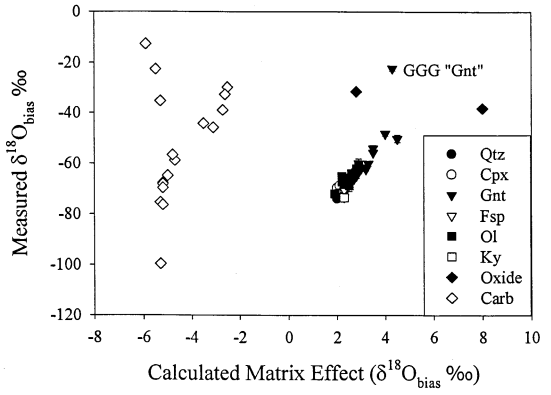

Fig. 23. Correlation between $\delta^{18}O_{bias}$ values measured on silicates, carbonates, oxide minerals, and a synthetic Gd–Ge–Ga garnet (GGG) and those predicted by using the kinetic energy sputtering model [29]. Abbreviations after Fig. 9.

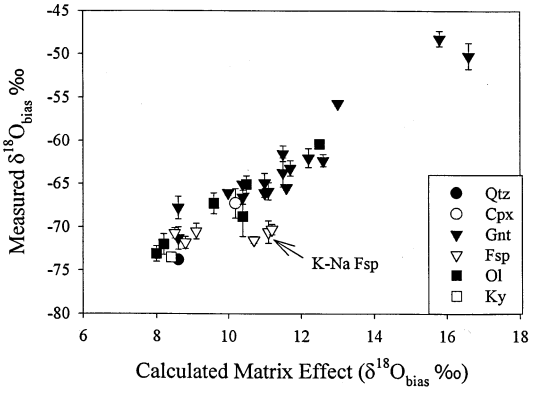

Fig. 24. Correlation between $\delta^{18}O_{bias}$ values measured on silicates and those predicted by using the kinetic energy sputtering model which includes Cs implantation estimated from $^{133}Cs^-/^{16}O^-$ secondary ion ratio. Abbreviations after Fig. 9. Error bars represent 1σ reproducibility.

that negative ionization potential (P^-) will be related to work function (ϕ) and electron affinity (A_o) according to the equation

$$P^- \propto \exp\left[-(\phi - A_o)/\epsilon_o\right] \quad (9)$$

Experimental work has demonstrated that ϵ_o is correlated with secondary ion emission velocity (v) for high energy ions [52], suggesting that ionization potential will follow the dependence

$$P^- \propto \exp\left[-(\phi - A_o)/v\right] \quad (10)$$

This indicates that a decrease in the work function due to increased Cs concentration will result in a decrease in the relative difference in ionization potential between the heavy and light isotope. Hence, the magnitude of the mass bias will also decrease with increasing Cs concentration. Although this is a potentially promising avenue for further investigation, it is complicated by difficulties in determining the work function in the chemically complex minerals of interest, especially after implantation by Cs.

Directly modeling the role of implanted Cs is problematic, as natural Cs is monoisotopic, and directly calibrating the Cs^- ion yield sputtered by $^{133}Cs^+$ primary ions would require the use of samples doped or implanted with highly radioactive ^{137}Cs. However, a semiquantitative attempt can be made by assuming an "average" Cs concentration. General limits can be placed by using (1) results of oxygen isotope ratio ($^{18}O/^{16}O$) depth profiles with an oxygen primary ion beam suggest that approximately two-thirds of the sputtered oxygen is derived from the primary beam, indicating that implanted Cs is ~50‰ of the sample, and (2) estimates of Cs^- ion yield by using those measured on other alkaline earth elements (Na and K) that suggest the implanted Cs is ~15–25‰ of the sample. By using the estimate from results of oxygen sputtering experiments as an upper limit, variations in the $^{133}Cs^-/^{16}O^-$ secondary ion ratios can be used to calculate the "amount" of Cs present in the sputtered volume if Cs ion yield is assumed to be constant for different silicate compositions (preliminary experiments based on Na and K suggest that it may actually vary by around 20–30‰). The estimated composition of the sputtered material, normalized to the original composition of the sample, can be used to calculate mass bias predicted by using the energy transfer model (Table 9, Fig. 24). The results by using this approach are mixed. The overall fit (assuming a linear model) is worse when compared to the fit obtained without considering Cs (r^2 of 0.80 compared to 0.87). Predicted mass biases are still heavy-isotope enriched, opposite to the measured light-isotope enrichment. However, inclusion of Cs increases the range of predicted mass bias by more than a factor of

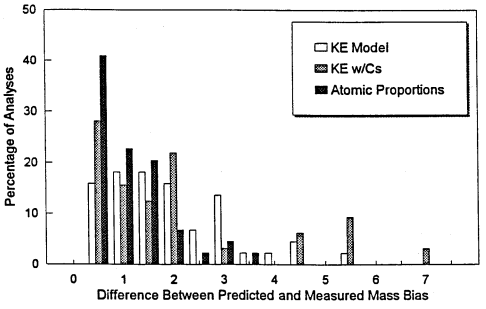

Fig. 25. Histogram of absolute differences (in 0.5‰ increments) between measured silicate mineral $\delta^{18}O_{bias}$ values and those predicted by using: (1) the kinetic energy (KE) model; (2) the KE model including estimated Cs contents; and (3) a model based on linear regression of atomic proportions of elements (see text, Table 9).

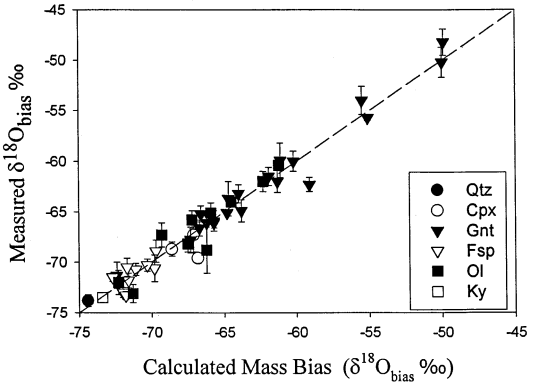

Fig. 26. Correlation between $\delta^{18}O_{bias}$ values measured on silicates and those predicted by using linear regression based on atomic proportions of cations. Abbreviations after Fig. 9. Error bars represent 1σ reproducibility.

three, resulting in much better agreement with the observed range of mass bias. Closer consideration of the data indicate that including Cs results in a higher percentage of predicted mass bias values that are within 2‰ of the measured values (Table 9, Fig. 25). Outliers from the general trend are mostly Na–K rich feldspars. Some of the deviation likely results from the use of a constant Cs^- ion yield in different silicates. These results suggest that, even though the proposed equation relating to the fundamental mechanism causing mass bias is incorrect, this model may still provide a reasonable empirical fit if Cs can be quantitatively incorporated.

The success of using end-member mineral components to model mass bias in some mineral groups led to investigation of the possibility that this empirical approach might work for silicates as a whole. Simple linear regression of major element chemistry against measured mass bias utilizing our silicate data set yields the best results we have obtained to date (Figs. 25 and 26; Table 9). With the exception of two samples, all predicted mass biases agree with the measured mass bias within 2σ of analytical error, and all but 3 of the 45 analyzed minerals have predicted $\delta^{18}O_{bias}$ values that are within 2‰ of the measured values. Reasonable results can also be obtained by using only Si, Mg, Ca, Fe, Mn, and Na concentrations, although with slightly greater scatter. A similar approach has been used effectively to predict hydrogen isotope mass bias in amphibole (a hydrous silicate) [10]. Although the oxygen mass bias results are purely empirical and are not based on any ionization model, the coefficients calculated for each element correlate with elemental properties including mass, electronegativity, and ionization potential, suggesting that future work relating calculated element-specific parameters to ionization models is warranted.

5.3. Carbon and oxygen mass bias in carbonates using high-energy secondary ions

The results of carbonate analyses provide additional insight into the relationship between chemical composition and mass bias, as a larger variation in major element chemistry is present in the carbonates compared to the silicates that have been studied. Overall, there are many similarities between mass bias behavior in silicates and carbonates, including correlations with atomic weight and relative mass bias behavior among near end-member composition standards. However, correlations between mass bias and secondary ion intensities of O and Cs vary. For silicates, little correlation is observed between oxygen ion yield and mass bias (Fig. 14), but there is good correlation between mass bias and the ratio of the secondary ion intensities of $^{133}Cs^-/^{16}O^-$ (Fig. 11). For reasons that are currently uncertain, the opposite

behavior is observed in carbonates (Figs. 18 and 19); there is a good correlation between oxygen yield and both carbon and oxygen mass bias, but poor correlation between mass bias and either $^{133}Cs^-/^{16}O^-$ or $^{133}Cs^-/^{12}C^-$ ratios. The carbonate mass bias variations indicate that there are important element- (or element group) specific dependencies. In general, relationships between ion yield, atomic weight, and mass bias indicate that the transition elements Fe, Mn, and Zn influence mass bias quite differently from that of the (mostly group II) elements Mg, Ca, Sr, Ba, and Pb. Furthermore, differences in the relative behavior of $\delta^{18}O_{bias}$ and $\delta^{13}C_{bias}$ in Zn carbonate indicates that certain elements vary in how they influence the measured isotope ratios of different elements. This suggests that there must be very element-specific characteristics that need to be incorporated into any sputtering model, even for high energy secondary ions.

The differences between Fe, Mn, and Zn carbonates and those of Mg, Ca, Sr, Ba, and Pb compositions are readily apparent when the kinetic energy sputtering model for predicting mass bias is applied to carbonates. For oxygen, a negative mass bias is predicted and observed (due to the presence of an element lighter than oxygen in the matrix), although only a 3‰ difference is predicted for compositions in which measured mass bias varied by 90‰ (Fig. 27). More critically, two distinct trends are observed in the data. For Fe–Mn–Ca solid solutions (and Zn-rich compositions), predicted and measured mass biases correlate fairly well, decreasing in a relatively systematic fashion from Ca-rich to Fe (Mn)-rich compositions, similar to behavior observed in silicates. However, Mg-rich compositions lie on a different trend, as do those for the heavier cations Sr, Ba, and Pb, for which the kinetic sputtering model predicts increasing mass bias whereas the measured mass bias actually decreases. For carbon isotopes, positive mass bias values are predicted, but negative mass bias values were measured. A difference of only 3‰ in $\delta^{13}C_{bias}$ is predicted between different compositions whereas differences of 40‰ have been measured (Fig. 27). As with oxygen isotopes, the correlation observed for transition metals breaks down when

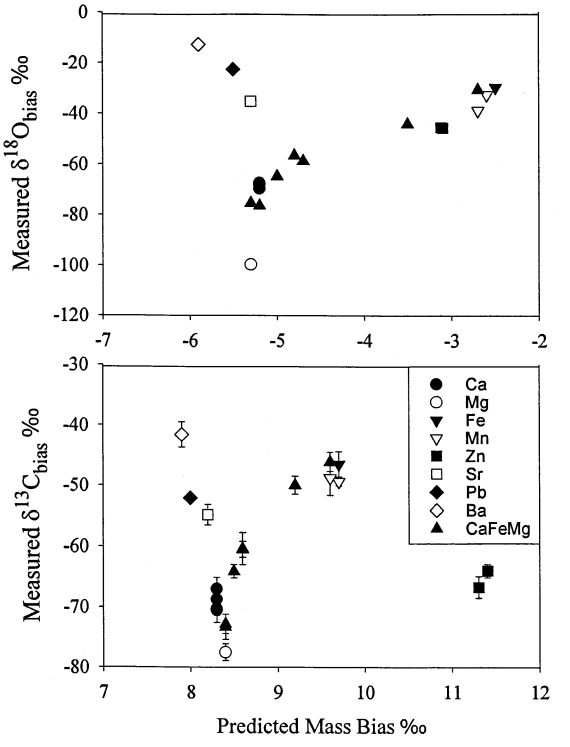

Fig. 27. Correlation between $\delta^{18}O_{bias}$ and $\delta^{13}C_{bias}$ values measured on carbonates and those predicted by using the kinetic energy sputtering model [29]. Abbreviations after Fig. 15. Error bars represent 1σ reproducibility.

other cations are considered and Zn-carbonate plots in a separate field on the carbon mass bias plot. These relationships are consistent when using atomic, ionic, or covalent radii, indicating that the kinetic energy mass bias model as currently formulated does not even qualitatively predict mass bias behavior across a wide range in chemical compositions. It is interesting to note that carbon ion yield (Fig. 20) correlates with the two trends observed in the energy transfer model for oxygen; predicted mass bias values for Fe–Mn–Zn compositions fall along a different trend compared to other carbonates, similar to correlations observed between $\delta^{18}O_{bias}$ and C ion yield. With the exception of Zn carbonate, similar relations are present for carbon isotopes as well.

The $\delta^{13}C_{bias}$ value for graphite is −46.5‰, an intermediate value compared to the carbonates, even though it has the lightest atomic mass. The $\delta^{13}C_{bias}$

value expected based on the $Mass_{light}/Mass_{heavy}$ relation observed for pure metals [43] is −78‰, a value similar to that measured on $MgCO_3$, but much greater than that measured on the pure target. These results are additional evidence that there are other influences on matrix effects for high energy ions in addition to those incorporated into the energy transfer model (efficiency of the energy transfer during collision, mass, and radius of atoms in the matrix).

5.4. Oxygen isotope mass bias in silicates and carbonates using low-energy secondary ions

Recently, high precision (∼1‰) $\delta^{18}O_{bias}$ measurements in silicate minerals were obtained for low-energy secondary ions. These experiments were carried out by using VG Isolab [4,47,49,53] and Cameca 1270 [5,48] instruments. Compared with the Cameca 3f and 4f series instruments, the Cameca 1270 is equipped with a redesigned electron gun that is easier to align and delivers a more homogeneous electron cloud, allowing more stable charge compensation and utilization of low energy secondary ions for isotope ratio measurements in insulators. The use of low-energy secondary ions results in higher secondary ion count rates for a given primary beam current even when using high mass resolution. Although only a small number of minerals have been analyzed, it is apparent that both the absolute magnitude of the mass biases and their range are considerably smaller. For Mg-rich olivines $\delta^{18}O_{bias}$ values are in the 0 to −5‰ range for measurements made on both the Cameca 1270 and the VG Isolab. Matrix effects in olivine are significantly reduced over the compositional range of 100‰ to 80‰ Mg_2SiO_4; $\delta^{18}O_{bias}$ values change <4‰ for low energy ions [54] as compared to a ∼12‰ shift in $\delta^{18}O_{bias}$ values for extreme energy filtering. Measurements made on other minerals (quartz, feldspar, spinel, pyroxene) indicate that $\delta^{18}O_{bias}$ corrections are typically only a few per mil [55,54]. Currently, there is insufficient data to determine if there are systematic correlations between mass bias measured by using low energy ions and matrix composition.

Although limited to Ca–Mg–Fe solid solutions, measurements of oxygen isotope mass bias in carbonates by using low-energy secondary ions have been made [45,46]. These results suggest that mass bias variations measured by using low-energy ions are more complex compared to those measured by using high-energy ions. For the Cameca 1270, $\delta^{18}O_{bias}$ values were −2‰ for calcite ($CaCO_3$), −10‰ for siderite ($FeCO_3$), −9‰ for dolomite [$MgCa(CO_3)_2$], and −16‰ for magnesite ($MgCO_3$) [48]. This 14‰ range in mass bias compares to a ∼80‰ range observed by using high energy ions. Although the data set is very limited, it suggests that mass bias might be fairly linear as a function of atomic Mg along the Ca–Mg binary join for low energy ions. However, the mass bias of the Fe carbonate lies between that of Ca and Mg carbonate, in contrast to the general correlation between mass bias and atomic mass observed for high-energy ions, suggesting that matrix effects in multicomponent solid solutions may be less systematic for low energy ions. Matrix effects in carbonates measured by using low-energy ions on a VG Isolab are substantially different: $\delta^{18}O_{bias}$ values around 0‰ for Mg and Fe end members, +17 to +18‰ along the $(FeMg)Ca(CO_3)_2$ join, and approximately the same value (+19‰) for the calcium end member [46]. These values do not appear to vary linearly along binary joins or with atomic mass. The measured mass biases in both data sets do not correlate with bond energies, electronegativity, or ionization potentials.

These results suggest that the use of low-energy ions has both advantages and disadvantages when compared to high-energy ions. Ion yields are higher, leading to shorter analysis times, better spatial resolution, and potentially better precision. The magnitude of matrix effects is three to five times smaller for low-energy secondary ions, so the absolute magnitude of the bias correction is smaller. However, results to date suggest that matrix effects may be more complex and less systematic for low-energy secondary ions, making it more difficult to obtain accurate analyses where standards and samples are not closely matched. There may be additional factors complicating the use of low energy ions: mineral orientation has been shown to change the measured mass bias by several

per mil for both oxygen isotopes [51] in magnetite and hydrogen isotopes [11] in hydrous silicate and hydroxide minerals. In addition, mass bias for sulfur measured by using low-energy ions has been observed to vary by up to 8‰ between different sample mounts containing different pieces of the same standard [16,17]. No such mass bias difference has been observed by using high energy ions. All of these problems suggest that, high ion yields notwithstanding, improving the accuracy of analyses for low-energy ions beyond current capabilities obtained with high energy ions in chemically variable matrices may be difficult.

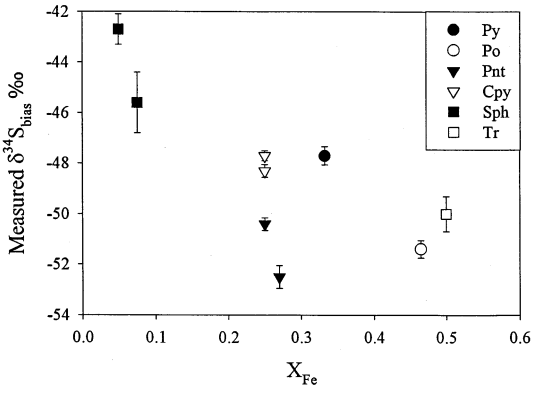

Fig. 28. Measured $\delta^{34}S_{bias}$ sulfides values for high energy secondary ions as a function of the proportion of atomic Fe. Abbreviations after Fig. 5. Error bars represent 1σ reproducibility.

5.5. Sulfur isotopes

Although sulfur isotope ratio measurements by SIMS are relatively routine, little work has been done to develop predictive mass bias models. This is in part because many sulfide minerals are isochemical and thus standardization is relatively simple. In addition, the range of mass bias observed by using Cs^+ primary ions and negative secondary ions is small (3–8‰, depending on secondary ion energy) compared to large ranges (10–100‰) measured for O and C isotopes.

The results for both positive and negative secondary ions suggest that use of a Cs^+ primary ion beam minimizes the magnitude of the matrix effect on mass bias (Fig. 6), as well as resulting in higher ion yields (Fig. 4). If variable chemical enhancement due to implantation of the sputtering species was the dominant factor, one would predict that use of an oxygen primary ion beam would enhance ion yields and minimize matrix effects for positive secondary ions and Cs would minimize matrix effects for negative secondary ions. For positive secondary ions, the relative difference in sulfur ion yield between different minerals is much smaller when using an oxygen primary ion beam other than Cs^+ (Fig. 4). This fits with predicted behavior, as oxygen flooding is often used to minimize ion yield differences. However, this minimization of ion yield differences does not extend to isotope effects. Although the largest difference in positive ion yields between minerals is observed by using a Cs^+ primary ion beam, Cs minimizes differences in $\delta^{34}S_{bias}$ values by using both positive and negative secondary ions. This implies that the effect of chemical enhancement due to oxidation [e.g. 35] for positive secondary ions does not play the primary role in controlling mass bias effects. Compared to low energy secondary ions, use of high-energy, negative secondary ions (sputtered with Cs^+ primary ions) decreases differences in relative ion yield between different minerals, but the difference in mass bias increases. The differences of ion yield and mass bias behavior as a function of secondary ion energy suggest that mass bias and ion yield are somewhat decoupled; although differences in sulfur ion yield as a function of matrix composition decrease with increasing ion energy, the difference in ion yield between sulfur isotopes increases.

Although the small absolute variations in $\delta^{34}S_{bias}$ values between different minerals makes it difficult to quantify mass bias relations, the mass bias behavior of high-energy negative secondary ions appears to be more systematic than those of low-energy ions. There seems to be a correlation between increasing proportion of atomic iron and increasing mass bias (Fig. 28), a trend opposite to that observed for oxygen and carbon isotopes in silicates and carbonates. There is also a correlation between decreasing mass bias and increasing sulfur ion yield (Fig. 29), similar to the correlation observed for increasing oxygen ion yield

and decreasing oxygen (and carbon) mass bias in carbonates. Application of the kinetic energy mass bias model yields a poor correlation between predicted and observed mass bias (Fig. 30).

Thus far, correlation of mass bias behavior for low-energy sulfur ions with other parameters has been difficult. As variations in $\delta^{34}S_{bias}$ values measured by using the Cs^+ primary beam are not much larger than the total analytical error (SIMS + conventional determination), testing for correlations is problematic. Due to the much larger range in $\delta^{34}S_{bias}$, this is not a problem for analyses obtained by using oxygen primary beams. There are no apparent correlations between mass bias and ion yield, bond strength, mean electronegativity, ionization potential, and chemical composition for low-energy secondary ions.

6. Summary and conclusions

In the past few years, great strides have been made in improving the precision and accuracy of SIMS light stable isotope ratio measurements. The precision and reproducibility of such analyses is virtually identical to the theoretical counting statistical limit, and the demonstrated precision of SIMS analyses is approaching that of conventional techniques for some elements (Table 1). These capabilities are opening new areas of geochemical and cosmochemical research in a wide range of geologic settings. In many cases, the limits of SIMS applicability are more often due to problems in accuracy arising from matrix effects, rather than precision of the analysis.

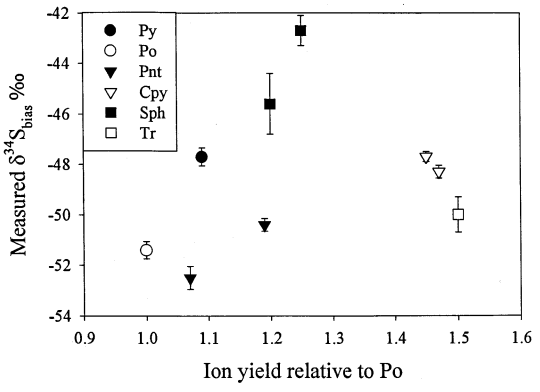

Fig. 29. Measured $\delta^{34}S_{bias}$ sulfides values for high energy secondary ions as a function of sulfur ion yield (normalized to pyrrhotite). Abbreviations after Fig. 5. Error bars represent 1σ reproducibility.

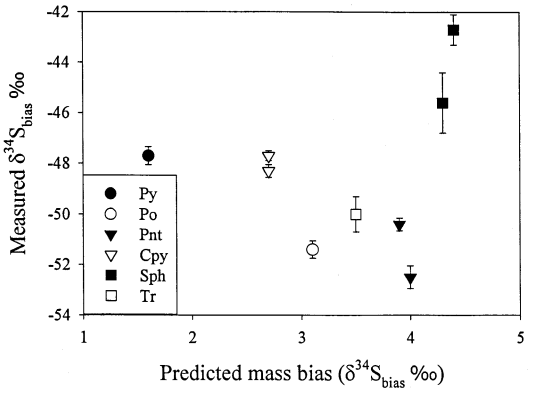

Fig. 30. Relationship between measured and predicted (kinetic sputtering model) $\delta^{34}S_{bias}$ values for high energy secondary ions. Abbreviations after Fig. 5. Error bars represent 1σ reproducibility.

Available oxygen isotope data measured by using high-energy secondary ions indicates that there are predictable correlations between mass bias, matrix composition, and fundamental characteristics of the elements composing the sample. Empirical models based on chemical composition produce relatively accurate predictions of mass bias in silicates. For individual mineral groups, modeling mass bias as a linear function of chemical composition has proved successful (e.g. Mg-rich olivines, garnets). However, this approach requires use of multiple standards spanning the compositional range of interest, as mass bias is not always accurately predicted by using a linear function based on mineral composition (e.g. carbonates. For all silicates, good results are obtained by using a linear equation based on the atomic proportion of cations in the matrix; for >95‰ of the minerals analyzed, the predicted and measured mass bias on each mineral agree within 2σ of the analytical error.

A theoretical model predicting mass bias for high energy secondary ions, based on the efficiency of kinetic energy transfer during the collision process, has been proposed [27]. The general trend of mass bias predicted by using this model is consistent with measured mass bias in silicate minerals, although

inaccuracies of up to 5‰ would result if applied to the data presented here. However, the model predicts mass bias favoring the heavy isotope, whereas measured mass biases favor the light isotope. In addition, the magnitude of mass bias variations between different matrices is far smaller than observed variations. Application of this model to oxides and carbonates produces inconsistent results, and fails to predict trends for carbon and sulfur isotopes in carbonates and sulfides, respectively. These results suggest that the proposed energy transfer model is not accurately formulated to reflect the mechanisms causing mass bias for high energy ions. However, characteristics of the energy transfer model as currently formulated mimic those that would lead to variations in the amount of Cs in the sputtered volume. Our results indicate that mass bias in silicates is well correlated with $^{133}Cs^-$ secondary ion intensity. It may be that the limited success of the energy transfer model actually reflects the amount of Cs in the sputter volume and that Cs implantation is a major factor controlling mass bias.

Mass bias behavior of low-energy secondary ions appears to vary significantly depending on the element whose ratio is measured. Although matrix effects are very large, systematic correlations are observed between bond energy proxies, mineral chemistry, and hydrogen mass bias measured by using an O^- primary ion beam and positive secondary ions [10,11], and hydrogen mass bias can be successfully predicted by using empirical calibrations based on major element ion yield [10]. Although the reasons are presently unclear, there does not appear to be any matrix effect for boron isotope ratios measured by SIMS, and a universal correction can be applied to both minerals and solutions [9]. Mass bias for either positive or negative low-energy secondary sulfur ions does not appear to be strongly correlated with any obvious matrix-related factors. Currently, there is insufficient data to predict the pattern of oxygen isotope matrix effects for low-energy ions. Although overall matrix effects are smaller for low-energy ions when compared to high-energy ions, there are indications from carbonates that matrix effects may not be directly correlated to fundamentals of mineral composition such as average atomic weight.

Presently, utilization of either high- (extreme energy filtering) or low-energy (high mass resolution) secondary ions has both advantages and disadvantages. The relationship between mass bias and matrix composition appears to be more systematic with extreme energy filtering, making matrix corrections when closely matched standards are not available potentially simpler. For extreme energy filtering, instrumental tuning is simpler, sample charging is less problematic, and the technique appears to be less sensitive to surface-related effects. With present calibration methods, it is possible to predict mass bias with accuracy that is within 1–2 times the precision of the analysis for a variety of mineral compositions, making practical application possible to a variety of minerals. However, it is unlikely that significant increases in precision of the extreme energy filtering technique will occur with present instrumentation, as there is no simple way to improve ion yields. For low-energy ions, both the magnitude and the variation in mass bias as a function of matrix composition are 2–5 times smaller than those observed by using high-energy ions. Ion yields are 5–100 times greater for low-energy ions, improving potential precision, spatial resolution, and analysis time. However, mineral orientation is reported to have a significant effect on mass bias when analyzing hydrogen isotopes in a number of minerals and oxygen isotopes in magnetite [11,53], and mass bias for low energy sulfur ions has been observed to vary significantly between different sample mounts [16,17]. The much higher ion yields available by using low-energy ions indicate that it may be possible to achieve precision on 10–30 μm spots that essentially matches that of conventional techniques, particularly if multicollector detector systems can be improved. However, in parallel to any improvements in the precision, there is a clear requirement for a more complete understanding of matrix-dependent effects in chemically complex natural materials.

Acknowledgements

Research sponsored by the ORNL Laboratory Director's Research and Development Program and the Office of Basic Energy Science, U.S. Department of Energy, under contract no. DE-AC05-96OR22464 with Oak Ridge National Laboratory, managed by Lockheed Martin Energy. Additional support came from NSF grant nos. EAR-95-27567 and EAR-97-06077 and NASA grant nos. NAGW 2800 and NAGW 3621. B.A.P. and R.L.R. were also sponsored by ORAU/ORISE. We would like to thank Larry Anovitz, Adrian Boyce, Dave Cole, John Craven, Doug Crowe, Dave Lowry, Calum Macaulay, Claudia Mora, Larry Taylor, Clive Neal, Zach Sharp, and John Valley for help in acquiring or analyzing standards, and Dave Smith, Jim Delmore, and an anonymous reviewer whose comments and suggestions greatly improved the manuscript. We would also like to gratefully thank Ian Lyon and Kevin McKeegan for providing data on oxygen mass bias measured by using low energy secondary ions.

References

[1] L.R. Riciputi, D.R. Cole, H.G. Machel, Geochim. Cosmochim. Acta 60 (1996) 325.
[2] J.P. Greenwood, L.R. Riciputi, H.Y. McSween Jr., Geochim. Cosmochim. Acta 61 (1997) 4449.
[3] R.L. Hervig, L.B. Williams, I.K. Kirkland, F.J. Longstaffe, Geochim. Cosmochim. Acta 59 (1995) 2537.
[4] I.C. Lyon, J.M. Saxton, P.J. McKeever, E. Chatzitheodoridis, P. Van Lierde, Int. J. Mass Spectrom. Ion Processes 9 (1995) 1.
[5] L.A. Leshin, A.E. Rubin, K.D. McKeegan, Geochim. Cosmochim. Acta 61 (1997) 835.
[6] E. Deloule, F. Allegre, S.M.F. Sheppard, Earth Planet. Sci. Lett. 105 (1991) 543.
[7] J.M. Eiler, J.W. Valley, C.M. Graham, L.P. Baumgartner, Contrib. Mineral. Petrol. 118 (1995) 365.
[8] N. Shimizu, S.R. Hart, Annu. Rev. Earth Planet. Sci. 10 (1982) 483.
[9] M. Chaussidon, F. Robert, D. Mangin, P. Hanon, E.F. Rose, Geostand. Newslett. 21 (1997) 7.
[10] E. Deloule, C. France-Lorand, F. Allegre, in Stable Isotope Geochemistry, Geochemistry Society Special Publ. H.P. Taylor Jr., J.R. O'Neill, I.R. Kaplan (Eds.), 3, 1991.
[11] L.R. Riciputi, T. Chacko, D.R. Cole, J. Horita, Analysis of hydrogen isotope ratios by SIMS, and application to determining mineral-fluid isotope fractionation factors, in G. Gillen, R. Lareau, J. Bennett, F. Stevie (Eds.), Secondary Ion Mass Spectrometry, SIMS XI, Wiley, New York, 1998, pp. 79–82.
[12] E. Deloule, C. Allegre, B. Doe, Econ. Geol. 81 (1986) 1307.
[13] R.L. Hervig, P. Williams, R.M. Thomas, S.N. Schauer, I.M. Steele, Int. J. Mass Spectrom. Ion Processes 120 (1992) 45.
[14] J.B. Metson, G.M. Bancroft, N.S. McIntyre, W.J. Chauvin, Surf. Int. Anal. 5 (1983) 181.
[15] L.R. Riciputi, B.A. Paterson, Am. Mineral. 79 (1994) 1227.
[16] L.R. Riciputi, Rapid Commun. Mass Spectrom. 10 (1996) 282.
[17] B.A. Paterson, L.R. Riciputi, H.Y. McSween Jr., Geochim. Cosmochim. Acta 61 (1997) 601.
[18] M.L. Jensen, N. Nakai, in Biogeochemistry of Sulfur Isotopes, M.L. Jensen (Ed.), NSF Symp. Vol. 1962.
[19] P. Baertschi, Earth Planet. Sci. Lett. 31 (1976) 341.
[20] G. Hut, Consultant's Group Meeting on stable isotope reference samples for geochemical and hydrologic investigations, IAEA, Vienna, 16–18 September 1985, Report to the Director General, IAEA, Vienna, p. 42.
[21] T.L. Zhang, L. Wenjun, Proc. 2nd Beijing Conf. and Exhib. on Instrum. Analysis (1987) 391.
[22] C.S. Eldridge, W. Compston, I.S. Williams, J.L. Walshe, R.A. Bothe, Int. J. Mass Spectrom. Ion Processes 54 (1987) 40.
[23] M. Chaussidon, F. Albarede, M.F. Sheppard, Nature 330 (1987) 242.
[24] M. Chaussidon, J.-P. Lorand, Geochim. Cosmochim. Acta 54 (1990) 2835.
[25] A.W. Macfarlane, N. Shimizu, Geochim. Cosmochim. Acta 55 (1991) 525.
[26] S.N. Schauer, R.T. Lareau, R.L. Hervig, P. Williams, In Secondary Ion Mass Spectrometry-SIMS IX, A. Benninghoven, Y. Nihei, R. Shimizu, H.W. Werner (Eds.), Wiley, New York, 1994.
[27] H. Gnaser, I.D. Hutcheon, Phys. Rev. B 35 (1987) 877.
[28] E.U. Engstrom, A. Lodding, H. Odelius, U. Sodervall, Mikrochim. Acta (1987) 387.
[29] J.M. Eiler, C. Graham, J.W. Valley, Chem. Geol. 138 (1997) 221.
[30] J.W. Valley, J.M. Eiler, C.M. Graham, E.K. Gibson, C.S. Romanek, E.M. Stolper, Science 275 (1997) 1633.
[31] J.M. Schroeer, T.N. Rhodin, R.C. Bradley, Surf. Sci. 34 (1973) 571.
[32] N.H. Gries, F.G. Ruedenauer, Int. J. Mass Spectrom. Ion Phys. 18 (1975) 111.
[33] P. Williams, Surf. Sci. 90 (1979) 588.
[34] H. Gasner, H. Oechsher, Nucl. Instrum. Methods Phys. Res. B 48 (1990) 544.
[35] M.L. Yu, N. Lang, Nucl. Instrum. Methods Phys. Res. B 14 (1986) 403.
[36] G. Slodzian, J.C. Lorin, A. Havette, J. Phys. 23 (1980) 555.
[37] W.F. Van Der Weg, D.J. Bierman, Physica 44 (1969) 206.
[38] M.L. Yu, Phys. Rev. Lett. 47 (1981) 1325.
[39] M.J. Vasile, Surf. Sci. 115 (1982) L141.
[40] M.L. Yu, K. Mann, Phys. Rev. Lett. 57 (1986) 1476.
[41] G. Slodzian, in Secondary Ion Mass Spectrometry-SIMS III, A. Benninghoven (Ed.), Springer, 1982.

[42] U. Sodervall, E.U. Engstrom, H. Odelius, A. Lodding, in Secondary Ion Mass Spectrometry-SIMS VI, A. Benninghoven, A.M. Huber, and H.M. Werner (Eds.), Wiley, New York, 1988.
[43] N. Shimizu, S.R. Hart, J. Appl. Phys. 53 (1982) 1303.
[44] E.C. Goldberg, J. Ferron, M.C.G. Passeggi, in Secondary Ion Mass Spectrometry-SIMS VI, A. Benninghoven, A.M. Huber, H.M. Werner (Eds.), Wiley, New York, 1988.
[45] L.R. Riciputi, B.A. Paterson, in 5th V.M. Goldschmidt Program and Abstracts, H.G. Barnes (Ed.), Penn. State University, 1995.
[46] L.R. Riciputi, B.A. Paterson, Eight Annual Workshop on Secondary Ion Mass Spectrometry, Lake Poconos, 1995.
[47] J.M. Saxton, I.C. Lyon, E. Chatzitheodoridis, I.K. Perera, P. van Lierde, P. Freedman, G. Turner, Int. J. Mass Spectrom. Ion Processes 154 (1996) 99.
[48] L.A. Leshin, K.D. McKeegan, P.K. Carpenter, R.P. Harvey, Geochim. Cosmochim. Acta 62 (1998) 3.
[49] J.M. Saxton, I.C. Lyon, G. Turner, Meteor. Planet. Sci. 32 (1997) A114.
[50] W. Gerhard, C. Plog, in Secondary Ion Mass Spectrometry-SIMS VI, A. Benninghoven, A.M. Huber, H.M. Werner (Eds.), Wiley, New York, 1988.
[51] N.D. Lang, Phys. Rev. B 27 (1983) 2019.
[52] P.W.A. van der Heide, Surf. Sci. 365 (1996) 473.
[53] I.C. Lyon, J.M. Saxton, S.J. Cornah, Int. J. Mass Spec. Ion Proc. 172 (1998) 115.
[54] J.M. Saxton, I.C. Lyon, G. Turner, Analyst 120 (1995) 1321.
[55] J.C. Lorin, R. Slodzian, R. Dennebouy, M. Chaintreau, In Secondary Ion Mass Spectrometry-SIMS VII, A. Benninghoven, R.J. Colten, D.S. Simons, H.W. Werner (Eds.), Wiley, New York, 1990.
[56] J.M. Saxton, I.C. Lyon, G. Turner, Analyst 120 (1995) 1321.
[57] R.N. Clayton, T.K. Mayeda, Geochim. Cosmochim. Acta 27 (1963) 43.
[58] J.M. McCrea, J. Chem. Phys. 18 (1950) 849.
[59] J. Rosenbaum, S.M.F. Sheppard, Geochim. Cosmochim. Acta 50 (1986) 1147.
[60] H. Craig, Geochim. Cosmochim. Acta 3 (1953) 53.
[61] T.A. Raftler, New Zealand J. Sci. Technol. B 38 (1957) 849.
[62] D.E. Crowe, J.W. Valley, K.L. Baker, Geochim. Cosmochim. Acta 54 (1990) 2075.
[63] J. Bigeleisen, M.L. Perlman, H.C. Prosser, Anal. Chem. 24 (1952) 1356.
[64] J.D. Godfrey, Geochim. Cosmochim. Acta 26 (1962) 1215.
[65] E. Zinner, T. Ming, E. Anders, Geochim. Cosmochim. Acta 53 (1989) 3273.
[66] B. Harte, M.L. Otter, Chem. Geol. 101 (1992) 177.
[67] D.E. Crowe, R.G. Vaughn, Am. Mineral. 81 (1997) 187.